TI Designs

24-V$_{AC}$ Power Stage With Wide V$_{IN}$ Converter and Battery Gauge Reference Design for Smart Thermostats

Description
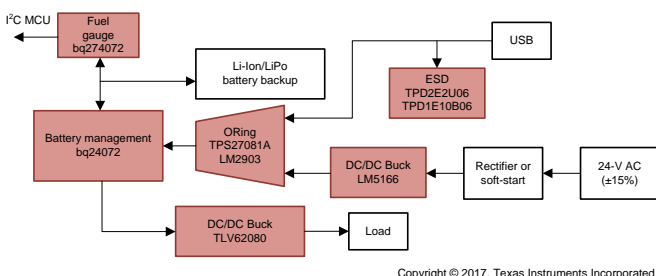
This TI Design provides a low BOM cost, high-efficiency power stage solution for smart thermostats, and other gateway building automation end equipment. This power stage takes a 24-V$_{AC}$ input and produces a 5-V and 3.3-V output rail, which can power additional point-of-load converters if added. The design provides LiPo battery charging and seamless switching to battery power during a 24-V$_{AC}$ brownout. The power-path capability provides battery power assistance allowing system load transient to exceed the current limit of the 24-V$_{AC}$ to DC system, allowing a lower cost wide V$_{IN}$ buck to be used. The battery fuel gauge helps designers preserve battery life and ensure proper operation by helping the central processor make smarter decisions on power saving and system functionality.

Resources

|	
TIDA-01395	Design Folder
LM5166	Product Folder
bq24072	Product Folder
TLV62080	Product Folder
BQ27426	Product Folder
TPS27081A	Product Folder
LM2903	Product Folder
TPD2E2U06	Product Folder
TPD1E10B06	Product Folder

ASK Our E2E Experts
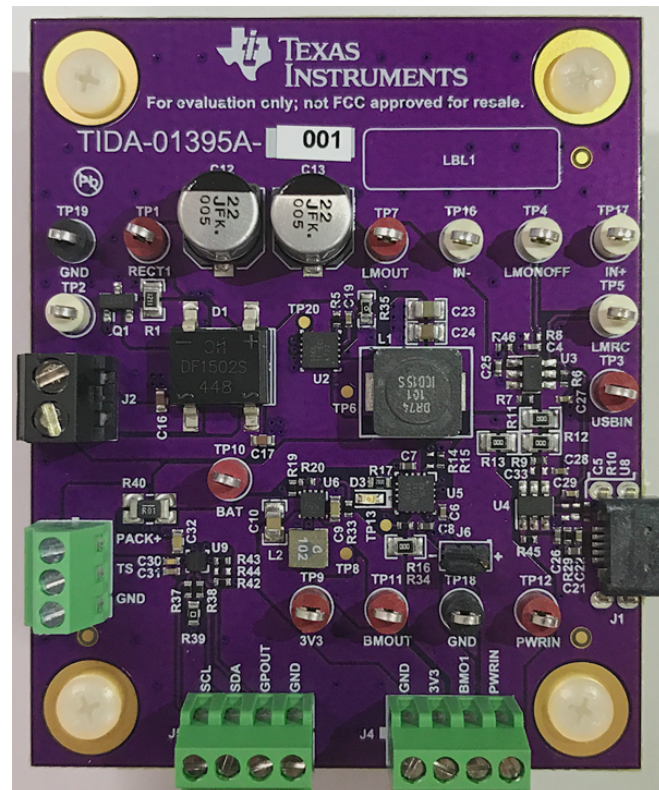
Features

- 24-V$_{AC}$ or USB to 3.3-V Power Rail
- Battery Backup
- Independent Battery Charging and Load Path
- Dynamic Power Path and Battery Power Assist
- High Efficiency Over Entire Load Current Range
- Battery Fuel Gauge Featuring Less Than 1% Error
- USB Overcurrent Compliant
- Discrete Solution

Applications

- Thermostat
- Video Doorbell
- Wireless Video Surveillance
- Gateway

Copyright © 2017, Texas Instruments Incorporated

24-V$_{AC}$ Power Stage With Wide V$_{IN}$ Converter and Battery Gauge Reference Design for Smart Thermostats

1

An IMPORTANT NOTICE at the end of this TI reference design addresses authorized use, intellectual property matters and other important disclaimers and information.

1 System Overview

1.1 System Description

A typical home uses a 24-V_{AC} system to power the HVAC system. Thermostats, as well as many other home automation equipment, use this 24-V_{AC} for power. Therefore, a power stage is needed to rectify the 24-V_{AC} and supply a DC voltage at the levels required by the thermostat's internal components. Low cost is typically a priority for thermostat designs as board space is often plentiful enough to avoid small-footprint, high-cost parts. For thermostats implementing a chargeable battery backup system, high efficiency also becomes a priority to allow a smaller, and therefore lower cost, battery to be used. The TIDA-01395 focuses on these priorities and can be easily adjusted to meet specific needs.

In addition to the 24-V_{AC} and battery backup, this TI Design allows a USB power supply to be used for charging and powering the system. Having two supply options, 24 V_{AC} and USB, requires an ORing device. ORing and power mux devices can be high in cost and therefore are avoided by designers; this TI Design provides a discrete based ORing solution that cuts costs significantly over fully featured integrated solutions. If a USB is not desired, the device can be removed with very minimal changes to the design.

The 24 V_{AC} is rectified and stepped down to a 5-V rail using an ultra-low I_Q, wide V_{IN}, 500-mA buck converter. The wide V_{IN} of the buck converter helps handle transients, thus eliminating the need for a TVS diode and other protection circuitry. Smaller capacitors may be used as the input voltage ripple can be higher when using a wide V_{IN} buck.
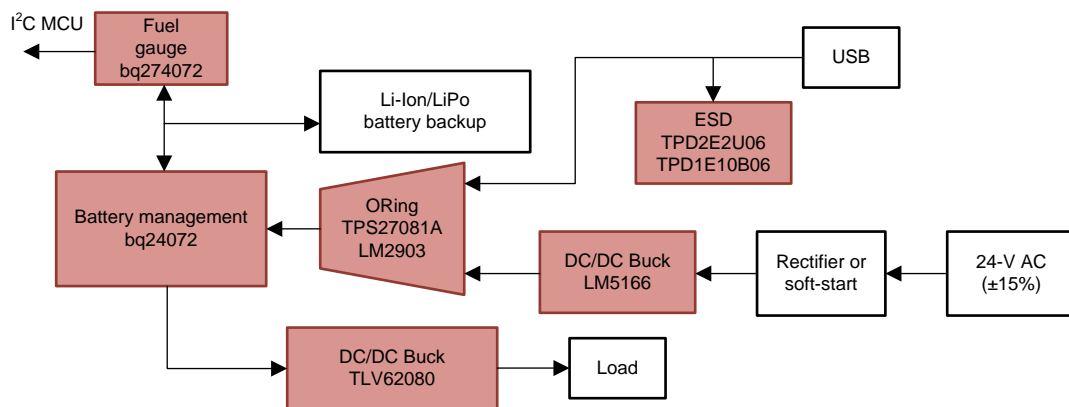
The TIDA-01395 uses a battery management device that allows independent current paths and monitoring for system power and battery charging. This device increases the cycle life of the battery. This TI Design features a seamless transition to battery power should the main supply fail, as well as battery power assist should the load requirement surpass the main supply's rating. Fuel gauging is also used to monitor the battery's state of charge (SOC) to ensure enough battery power is available for system operation. A very efficient, low cost, and low BOM count buck converter is used to step down the battery management voltage to 3.3 V for use by the general system. Both DC-DC buck converters in this design feature low-load power saving feature to provide high efficiency even at light loads.

1.2 Key System Specifications

Table 1. Key System Specifications

PARAMETER	SPECIFICATIONS	NOTES
Target application	Thermostat, gateway building automation	—
Main Input power source	20 V_{AC}	—
Secondary input power source	USB	—
LM5166 (RectOut to LMOut) efficiency	87.0%	160-mA output
TLV62080 (Battery to 3.3 V) efficiency	96.6%	160-mA output
LM5166 load regulation	1.41%	160-mA nominal output current and 24-V_{AC} nominal input voltage
TLV62080 load regulation	0.12%	160-mA nominal output current and nominal 3.7-V battery input
LM5166 max output current	500 mA	5-V bus
TLV62080 max output current	1 A	3.3-V bus
Working environment	Indoor	—
Form factor	52.324×64.262-mm rectangular PCB	—

1.3   Block Diagram

Figure 1. TIDA-01395 Block Diagram

1.4   Highlighted Products

Key features for selecting the devices for this reference design are highlighted in the following subsections. Find the complete details of the highlighted devices in their respective product datasheets.

1.4.1   LM5166

The LM5166 regulator is an easy-to-use synchronous buck DC/DC converter that operates from a 3.0- to 65-V supply voltage. The device is intended for step-down conversions from 5-V, 12-V, 24-V, and 48-V unregulated, semi-regulated and fully-regulated supply rails. With integrated high-side and low-side power MOSFETs, the LM5166 delivers up to 500-mA DC load current with exceptional efficiency and ultra-low input quiescent current in a very small solution size.

Designed for simple implementation, a choice of operating modes offers flexibility to optimize its usage according to the target application. Fixed-frequency, constant on-time (COT) operation with discontinuous conduction mode (DCM) at light loads is ideal for low-noise, high current, fast transient load requirements. Alternatively, pulse frequency modulation (PFM) mode achieves ultra-high, light-load efficiency performance. Control loop compensation is not required with either operating mode, reducing design time and external component count.

The LM5166 incorporates other features for comprehensive system requirements, including an open-drain Power Good circuit for power-rail sequencing and fault reporting, internally-fixed or externally-adjustable soft-start, monotonic startup into pre-biased loads, precision enable with customizable hysteresis for programmable line undervoltage lockout (UVLO), and thermal shutdown with automatic recovery. These features enable a flexible and easy-to-use platform for a wide range of applications. The pin arrangement is designed for simple and optimized PCB layout, requiring only a few external components.

The high-side p-channel MOSFET buck switch operates at 100% duty cycle in low dropout voltage conditions and does not require a bootstrap capacitor for gate drive.

In the TIDA-01395 design, the LM5166 serves to step down the rectified voltage from the 24-V_{AC} system to 5 V_{DC} for use by battery management system.

1.4.2 bq24072

The bq2407x series of devices are integrated Li-Ion sources linear chargers and system power path management devices targeted at space-limited portable applications. The devices operate from either a USB port or an AC adapter and support charge currents up to 1.5 A. The input voltage range with input overvoltage protection supports unregulated adapters. The USB input current limit accuracy and start up sequence allow the bq2407x to meet USB-IF inrush current specifications. Additionally, the input dynamic power management (V_{IN-DPM}) prevents the charger from crashing incorrectly configured USB wall adapters sources.

The bq2407x features dynamic power path management (DPPM) that powers the system while simultaneously and independently charging the battery. The DPPM circuit reduces the charge current when the input current limit causes the system output to fall to the DPPM threshold; thus, supplying the system load at all times while monitoring the charge current separately. This feature reduces the number of charge and discharge cycles on the battery, allows for proper charge termination and enables the system to run with a defective or absent battery pack.

1.4.3 TLV62080

The TLV6208x device focuses on high-efficiency step-down conversion over a wide output current range. At medium to heavy loads, the TLV6208x converter operates in PWM mode and automatically enters power save mode operation at light-load currents to maintain high efficiency over the entire load current range.

The TLV62080 synchronous switched-mode converters are based on DCS-Control™. DCS-Control is an advanced regulation topology that combines the advantages of hysteresis and voltage mode control.

Features:

- 2.5- to 5.5-V input voltage range
- 100% duty cycle for lowest dropout
- Power good output
- Power save mode for light load efficiency
- DCS-Control architecture for fast transient regulation

1.4.4 bq27426
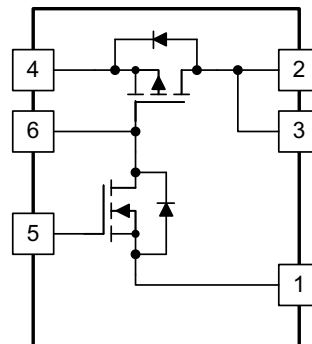
The bq27426 battery fuel gauge is a low-cost single-cell gauge that requires minimal user-configuration and system microcontroller firmware development, leading to quick system bring-up. The device features very low sleep power consumption, configurable interrupts, and accurate temperature sensing through an external thermistor. A low-value external sense resistor of 10 mΩ is used, allowing minimal power loss. The gauge resides on the system board, saving cost by eliminating the need for an additional PCB for a pack-side gauge.

bq27426 is based on Texas Instrument's patented Impedance Track™ Technology for increased accuracy that automatically adjusts for battery aging, self-discharge, temperature, and rate changes. The device reports remain capacity (mAh), SOC (%), battery voltage (mV), and estimates battery state of health (aging). A smoothing filter can be enabled to prevent transients from significantly affecting reported SOC.

1.4.5 TPS27081A

The TPS27081A device is a high-side load switch that integrates a Power PFET and a Control NFET in a small package. The TPS27081A device is capable fo handing up to 8 V and 3 A. To reduce voltage drop for low voltage and high current rails, the device implements an ultra-low resistance P-channel MOSFET, which reduces the dropout voltage through the device.

In the TIDA-01395 design, the TPS27081A device is used in conjunction with the LM2903 in a low-cost power ORing circuit to switch between the USB source and the LM5166 source.

Copyright © 2017, Texas Instruments Incorporated

Figure 2. TPS27081A Basic Schematic

1.4.6 LM2903

The LM2903 consists of two independent voltage comparators that are designed to operate from a single power supply over a wide range of voltages. This standard device has proven ubiquity and versatility across a wide range of applications. This is due to very wide supply voltages range (2 to 36 V), low I_Q and fast response of the devices.

The open-drain output allows the user to configure the output's logic low voltage (VOL) and can be used to enable the comparator to be used in AND functionality.

Features:
- Low output saturation voltage
- Maximum rating: 2 to 36 V
- Low input bias current: 25 nA (typical)
- Common-mode input voltage range includes ground

The LM2903 is used as the logic for the power ORing circuit in the TIDA-01395.

1.4.7 TPD2E2U06

The TPD2E2U06 is a dual-channel low capacitance TVS diode electrostatic discharge (ESD) protection device. The device offers ±25-kV contact and ±30-kV air-gap ESD protection in accordance with the IEC 61000-4-2 standard. The 1.5-pF line capacitance of the TPD2E2U06 makes the device suitable for a wide range of applications. Typical application interfaces are USB 2.0, LVDS, and I^{2}C.

Features:
- 5.5-A peak pulse current (8/29-µs pulse)
- Ultra-low leakage current 10 nA (max)
- Low ESD clamping voltage
- DC breakdown voltage 6.5 V (min)

The TPD2E2U06 is used on the USB communicated lines in the TIDA-01395.

1.4.8 TPD1E10B06

The TPD1E10B06 device is a single-channel 1 ESD transient voltage suppression (TVS) diode in a small 0402 package. This TVS protection product offers ±30-kV contact ESD, ±30-kV IEC air-gap protection, and has an ESD clamp circuit with a back-to-back TVS diode for bipolar or bidirectional signal support. The 12-pF line capacitance of this ESD protection diode is suitable for a wide range of applications supporting data rates up to 400 Mbps. The 0402 package is an industry standard and is convenient for component placement in space-saving applications.

Typical applications of this ESD protection product are circuit protection for audio lines (microphone, earphone, and speakerphone), SD interfacing, keypad or other buttons, VBUS pin and ID pin of USB ports, and general-purpose I/O ports. This ESD clamp is good for the protection of the end equipment like ebooks, tablets, remote controllers, wearables, set-top boxes, and electronic point of sale equipment.

The TPD1E10B06 is used to protect the USB VBUS pin on the TIDA-01395.

2   System Design Theory

The TIDA-01395 provides the main power stages needed for building automation electronics that are primarily powered from the 24-V_{AC} system used in typical homes. This TI Design presents a system solution that is modular in design, allowing system designers to easily modify the design if necessary to more closely match their product's specifications.

Cost reduction is a priority in this TI Design. Efficiency, particularly when using the battery backup, and heat loss are taken into consideration as well. To keep costs low, avoiding an over engineered system is required. The discrete nature of the TIDA-01395 allows designers to easily remove features they do not need, or easily add features and power rails that are required for their specific application.

This section outlines the theory and design considerations used to develop and design the TIDA-01395.

2.1   24-V_{AC} to DC Rectification

A full-bridge rectifier is used for DC rectification. To prevent a significantly large inrush current during initial connection of 24 V_{AC}, a soft-start circuit is implemented.

The schematic shown in Figure 3 shows the rectification and soft-start process. C1, C2, and C3 function as high frequency bypass capacitors. R1, R2, C4, and C5 provide the soft-start time constant for the gate of the N-channel MOSFET (T1). Q1 has a gate threshold voltage range of 1.0 to 2.5 V and a 92-mΩ $R_{DS(on)max}$ at V_{GS} = 10 V. The values of R_2 and R_3 are chosen to voltage divide a maximum of 42 V (the peak of the 24 V_{AC} at the high end of its tolerance) down to approximately 10 V once a steady state has been reached. Calculating R_2 and R_3 is shown in Equation 1:

$$42\,V\left(\frac{R_2}{R_2+R_3}\right)=42\,V\left(\frac{150\,k\Omega}{150\,k\Omega+453\,k\Omega}\right)=10.4\,V$$

(1)

Z1 is used as a protective device for the MOSFET gate. R4 is used to provide an initial current path while T1 is still open. The use of R4 prevents significantly differing soft-start times due to variances in the 24-V_{AC} transformer and Q1's gate threshold voltage. The resulting circuit provides a relatively consistent soft-start time regardless of the 24-V_{AC} source variances.

C6 and C7 function as the rectifier's smoothing capacitors. The TIDA-01395 has a maximum power output of 3.3 W. The output ripple will be a function of the load current. TINA-TI™ simulation shows a maximum worst case ripple of 11.7 V. This maximum assumes 4.3 W is required at the input to produce 3.3 W at the output and occurs when the 24-V_{AC} transformer is at the low-voltage edge of its tolerance and the output power of the 3.3-V rail is outputting its maximum current of 1 A. That worst case condition is typically unlikely to occur depending on application; a more reasonable use case of a 100-mA output from the 3.3-V rail and a nominal 24-V_{AC} transformer provides a rectification ripple of approximately 1.4 V. These ripple voltages must be checked in each application it is used. Even at the worse case scenario as previously outlined, the LM5166 buck converter is capable of handling those ripple voltages and voltage ranges.

Figure 4 shows a simulation example of the schematic detailed in Figure 3 under an input power of approximately 750 mW. The time from applied input power to the rectifier's output reaching steady-state is approximately 300 ms.
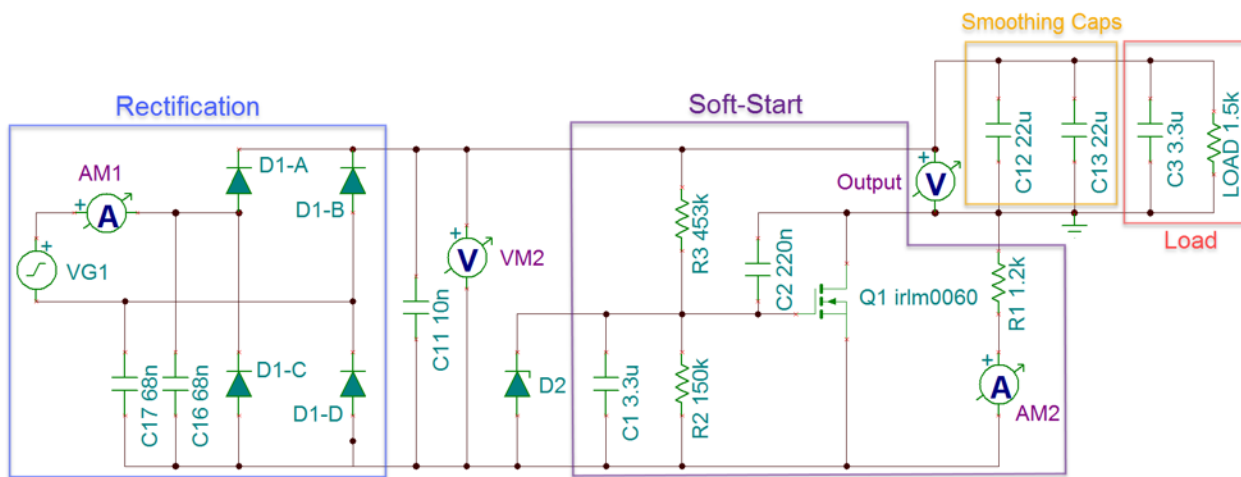

Figure 3. Soft-Start Schematic
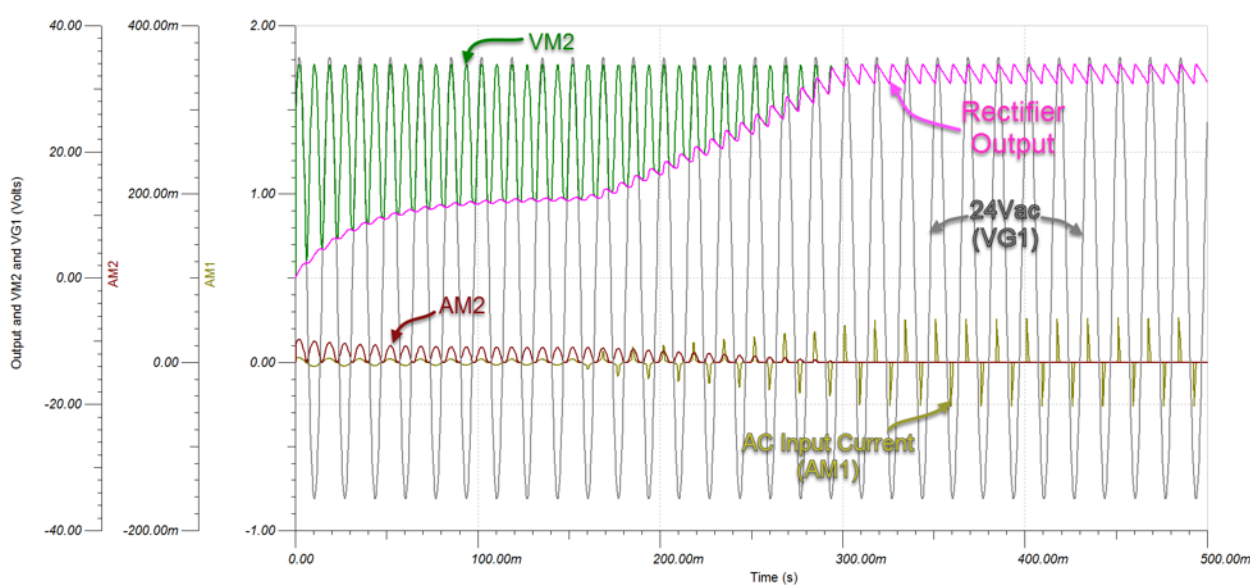
Figure 4. Soft-Start TINA-TI Simulation Example

8 *24-V_AC Power Stage With Wide V_IN Converter and Battery Gauge Reference Design for Smart Thermostats* TIDUCW0–March 2017

Submit Documentation Feedback
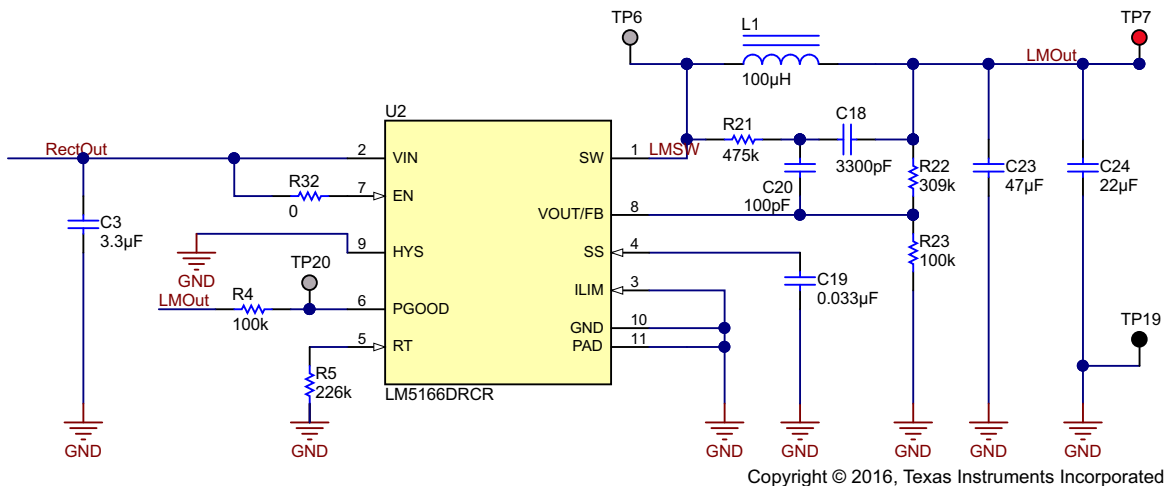
2.2 5-V Rails

This section provides detail on both the LM5166 wide V_{IN} buck that converts the rectified 24 V_{AC} to 5 V as well as the USB 5-V rail.

2.2.1 LM5166 Voltage Rail

The LM5166 is the optimal choice of device for this design. The device has a very wide input voltage range (3 to 65 V), yet it allows 500-mA loads and does so in a small package. It has an extremely low no-load quiescent current and high efficiency at light loads.

The LM5166 is used to convert the rectified 24-V_{AC} source to 5 V_{DC} and is used as the primary source of power in the TIDA-01395.

Copyright © 2016, Texas Instruments Incorporated

Figure 5. LM5166 Implementation

The TIDA-01395 uses the COT type III (COT III) method of the LM5166 to reduce the amount of output noise and ripple. Depending on the application, COT I, COT II, or PFM can be used to further reduce costs or quiescent current. However, a lower ripple will be more ideal for devices uses wireless technologies and systems needing reduced switching noise. To program the LM5166 to operate in COT mode, a resister, R5, is connected between the RT and GND pins. The value of R5 determines the switching frequency of the device per Equation 2. A low switching frequency of approximately 130 kHz will provide a higher efficiency.

$$R_5 = R_{RT}(k\Omega) = \frac{V_{OUT}(V)}{f_{sw}(kHz)} \times \frac{10^4}{1.75} = \frac{5.0\ V}{130\ kHz} \times \frac{10^4}{1.75} = 226\ k\Omega$$

(2)

The COT III ripple method uses a ripple injection circuit with R_{21}, C_{18}, and the switch node (SW) voltage to generate a triangular ramp. This triangular ramp is then AC-coupled into the feedback node (FB) with the capacitor C_{20}. Because this circuit does not use the output voltage ripple, it is suited for applications where low output voltage ripple is critical. Application note AN-1481[4] provides additional details on this strategy.

Datasheet recommendation for R_{23} is 10 to 100 kΩ for most applications. Higher resistance values are more susceptible to noise and therefore require a more careful PCB layout. In the TIDA-01395, R_{23} is chosen to be 100 kΩ and R_{22} is calculated using Equation 3. A value of 309 kΩ is conservatively chosen for R_{22}. Equation 4, Equation 5, and Equation 6 provide the value boundaries of C_{18}, C_{20}, and R_{21}. To stay within the calculated boundaries, 3300 pF is chosen for C_{18}, 475 kΩ for R_{21}, and 100 pF for C_{20}.

$$R_{22} = \frac{1.223\ V}{V_{OUT} - 1.223\ V} \times R_{23} = \frac{1.223\ V}{5 - 1.223\ V} \times 100\ k\Omega = 333\ k\Omega$$

(3)

$$C_{18} \geq \frac{5}{f_{sw} \times (R_{22} \| R_{23})} \Rightarrow C_{18} \geq \frac{5}{138\ kHz \times \left(\frac{309\ k\Omega \times 100\ k\Omega}{309\ k\Omega + 100\ k\Omega} \right)} \Rightarrow C_{18} \geq 480\ pF$$

(4)

$$C_{20} \geq \frac{1}{2\pi \times f_{SW} \times (R_{22} \| R_{23})} \Rightarrow C_{20} \geq \frac{1}{2\pi \times 138000 \times \left(\frac{309 \text{ k}\Omega \times 100 \text{ k}\Omega}{309 \text{ k}\Omega + 100 \text{ k}\Omega} \right)} \Rightarrow C_{20} \geq 15.3 \text{ pF}$$

(5)

$$R_{21}C_{18} \geq \frac{(V_{IN} - V_{OUT}) \times t_{on(@V_{IN})}}{20 \text{ mV}} \Rightarrow R_{21}C_{18} \geq \frac{(35 \text{ V} - 5 \text{ V}) \times \left(\frac{1}{138 \text{ kHz}} \times \frac{5 \text{ V}}{35 \text{ V}} \right)}{20 \text{ mV}} \Rightarrow R_{21}C_{18} \geq 1.553 \times 10^{-3}$$

(6)

The LM5166 prevents overcurrent conditions by cycle-by-cycle current limiting of the peak inductor current. The current sensed in the high-side MOSFET is compared every switching cycle to the current limit threshold set by the ILIM pin. When operating in COT mode, connecting the ILIM pin to GND will set a typical high-side FET current limit of 750 mA and low-side FET limit of 400 mA providing a maximum average DC current output of 500 mA.

The Enable pin is tied to V_{IN} and hysteresis is not used and thus tied to GND. Power good (PGOOD) is an open-drain output and is pulled up with a datasheet recommended 100-kΩ resistor R_4. The soft-start (SS) time can be programmable with an external capacitor C_{19} or left open for a default 900-µs soft-start time. An external capacitor was chosen for the TIDA-01395 to allow adjustability depending on application. Using Equation 7 and a desired soft-start time of approximately 4 ms provides a capacitance value of 0.033 µF for C_{19}.

$$C_{19} = C_{SS} (\text{nF}) = 8.1 \times t_{SS} (\text{ms}) = 8.1 \times 4 \cong 33 \text{ nF}$$

(7)

To calculate the value needed for L1, a desired inductor ripple current is needed. Knowing that the average DC output current is 500 mA while the peak inductor current cannot exceed 750 mA, the maximum ripple current allowed is 100% (inductor current swing from 250 to 750 mA providing a 500-mA total ripple). A more appropriate value for most applications is around 50%, 250-mA, inductor current ripple. A nominal inductance based on a 50% inductor current ripple is shown in Equation 8.

$$L1 = \frac{V_{LMOut}}{f_{SW} \times \Delta I_{L(nom)}} \times \left(1 - \frac{V_{LMOut}}{Rect_{Out}} \right) = \frac{5 \text{ V}}{138 \text{ kHz} \times 250 \text{ mA}} \times \left(1 - \frac{5 \text{ V}}{35 \text{ V}} \right) = 124 \text{ µH}$$

(8)

A lower value of 100 µH is chosen to improve efficiency and lower BOM size at the cost of additional inductor current ripple. The current ripple in this case is calculated in Equation 9 and the inductor current peak is subsequently calculated in Equation 10 and shows the peak stays within the 750-mA limit.

$$\Delta I_{L(nom)} = \frac{V_{LMOut}}{f_{SW} \times L1} \times \left(1 - \frac{V_{LMOut}}{V_{IN}} \right) = \frac{5 \text{ V}}{138 \text{ kHz} \times 100 \text{ µH}} \times \left(1 - \frac{5 \text{ V}}{35 \text{ V}} \right) = 311 \text{ mA}$$

(9)

$$I_{L1(peak)} = I_{OUT(max)} + \frac{\Delta I_{L(nom)}}{2} = 500 \text{ mA} + \frac{311 \text{ mA}}{2} = 656 \text{ mA}$$

(10)

Choose output capacitors C_{23} and C_{24} to satisfy Equation 11. Additionally, take into account the DC de-rating of the capacitors.

$$C_{Out} = C_{23} + C_{24} \geq \frac{\Delta I_{L(nom)}}{8 \times f_{SW} \times \Delta V_{LMOut}} \Rightarrow C_{23} + C_{24} \geq \frac{311 \text{ mA}}{8 \times 138 \text{ kHz} \times 20 \text{mV}} \Rightarrow C_{23} + C_{24} \geq 14 \text{ µF}$$

(11)
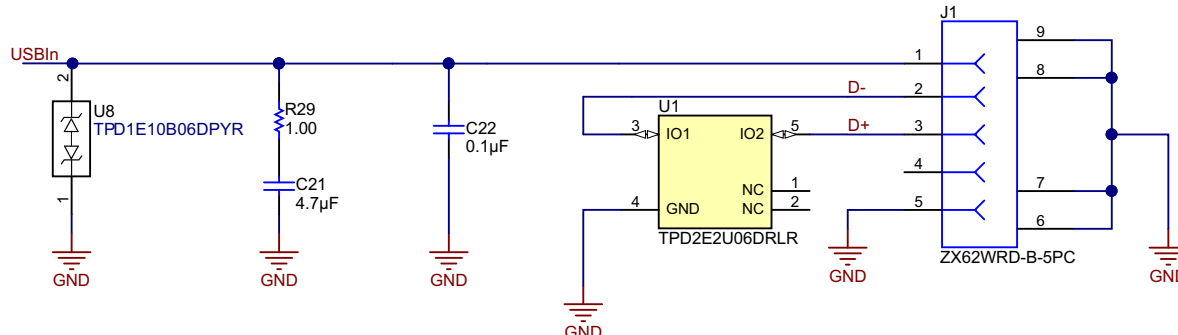
A total capacitance of 69 µF is chosen to account for tolerances and de-rating at 5 V.

2.2.2 USB Power Input

Like the LM5166, the USB power input is capable of powering the entire system. The USB can serve as a backup power source, be used for debugging other aspects of the product's systems, or be used to charge the battery should the main 24 V_{AC} not be available. The TIDA-01395 does not supply power to USB; it only sinks power from a USB host. ESD and overvoltage protection are included as shown in Figure 6.

This TI Design uses USB 2.0, and therefore assumes the max current that can pulled from a USB host is 500 mA. USB 2.0 specification allows a tolerance of 5% from the nominal 5 V, thereby giving a host voltage range of 4.75 5.25 V. Furthermore, USB 2.0 specification also allows the worst case voltage drop across all cables and connectors to bring the total voltage at load to 4.35 V. The TIDA-01395 is designed to accommodate USB 2.0 at its worst case specification.

R_{29} and C_{21} provide a snubber circuit to the USB Vbus, reducing the overshoot and ringing caused the cable inductance and capacitive load resonance. The snubber circuit must be tuned for each system design; therefore, the snubber component values used in the TIDA-01395 must be tested when designed into a new system and the values must be changed appropriately. The ORing circuit used in this TI Design has a maximum input voltage rating of 8 V, so the USB voltage must remain below that threshold and within USB specifications.

Copyright © 2017, Texas Instruments Incorporated

Figure 6. USB Implementation

2.3 Power Source ORing

The ORing section of the TIDA-01395 is designed to reduce costs while still allowing full system functionality from a USB power rail providing as little as 4.35 V.

A simple two-diode ORing configuration is not possible due to the voltage drop of forward biased diodes. The bq24072 battery management system used in this TI Design recommends a minimum of 4.35 V. USB 2.0 specifications allow the USB power bus to drop to 4.35 V at load. Therefore, there is virtually no margin available and thus basic diode oring cannot be used. A fully integrated power muxing chip is an option, though the costs are significantly higher and is thus avoided in this design. The ORing solution used in the TIDA-01395 uses two integrated N-FET/P-FET pairs and a basic comparator to accomplish power muxing capability at a significantly lower cost than a fully integrated solution.

As shown in Figure 7, U3 and U4 are TPS27081A chips, each containing an N-channel and P-channel MOSFET. U7, the LM2903, provides the basic logic necessary to accomplish the ORing. This ORing solution has the option to prioritize one source over another should both sources be available simultaneously by adjusting the voltage dividers on the comparator's input pins. Net "LMOut" Is connected to the 5-V output rail of the LM5166 while "USBIn" is connected to the USB power bus. The comparator, U7, is powered by the OUT (PWRin)_node. The parasitic diodes of the P-FETs on U3 and U4 provide an initial ORing method to power up the comparator until one of the switches is closed.
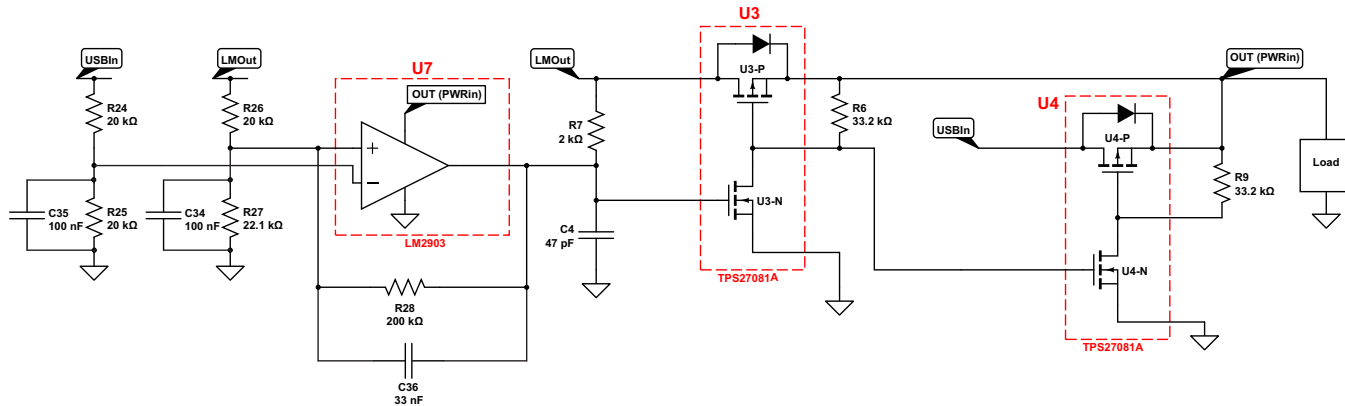
Figure 7. Power ORing Schematic

2.3.1 LMOut (LM5166) High

The 24-V_{AC} power, and consequently the LM5166 5-V rail, is considered the main power source for this system. If both power sources, USB and LMOut, are available and equal, the ORing will pass LMOut to the load. The voltage margin at which LMOut is prioritized over USB can be adjusted by choosing alternative values for R_{25}, R_{27}, and R_{28}. The margin, however, cannot be set higher than the forward voltage drop of the parasitic diodes of the P-FETs, as this could cause one of the P-FETs to latch closed or open during a brownout.

Figure 8 provides a visual overview of the functionality when the LM5166 is providing 5 V. The gate of the U3-N is pulled up through R7 to LMOut, thereby turning U3-N on and forcing the drain of the U3-N to GND. The drain of the U3-N is shorted to the gate of the U4-N. As a result, anytime U3-N is on, U4-N is off. U3-P is then turned on due to its gate being pulled to GND, and U4-P is turned off due to its gate being pulled up through R9. LMOut is then passed to the load.

The comparator's surrounding resistor values are chosen to ensure the non-inverting terminal will be higher than the inverting terminal if LMOut and USB is suppling 5 V, resulting in the comparator's output being Hi-Z and thus having virtually no effect on the circuit. This setup allows the LM5166 to dominate the ORing circuit over USB should the USB be plugged in when the LM5166 is already supplying power.
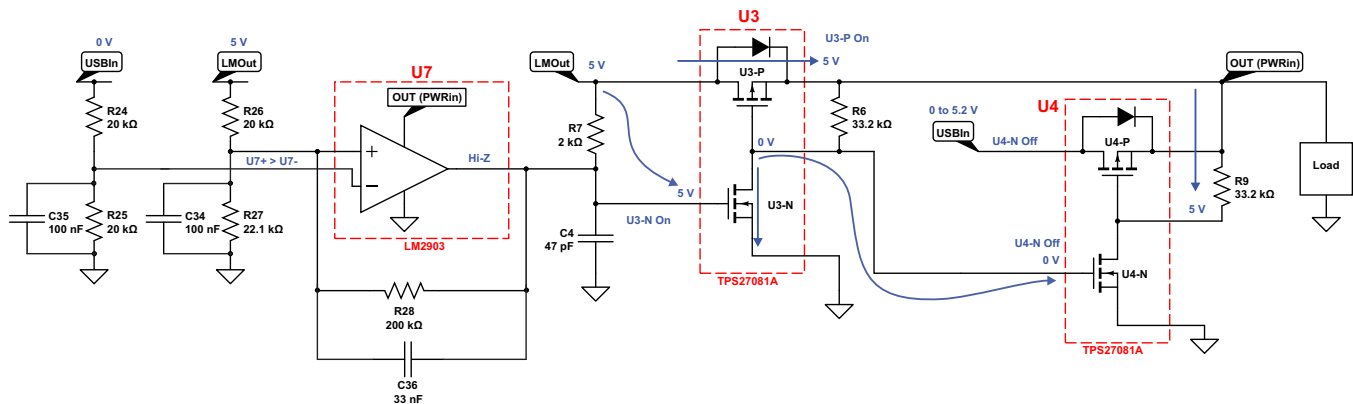
Figure 8. LM5166 Supplied Power ORing

2.3.2 USB While 24 V_{AC} is Absent

Figure 9 provides the visual overview of the ORing process when the USB is present and the 24-V_{AC} power line is absent. When Net "LMOut" is absent and "USBIn" is 4.35 to 5.25 V, the inverting input to the comparator becomes greater than the non-inverting input and the comparator drives the output terminal low, thereby turning off U3-N. With U3-N turned off, "USBIn" drives the gate of U4-N and the gate of U3-P high, turning off U3-P and turning on U4-N. U4-P will turn on as a result, and the USB voltage will be passed to the load.
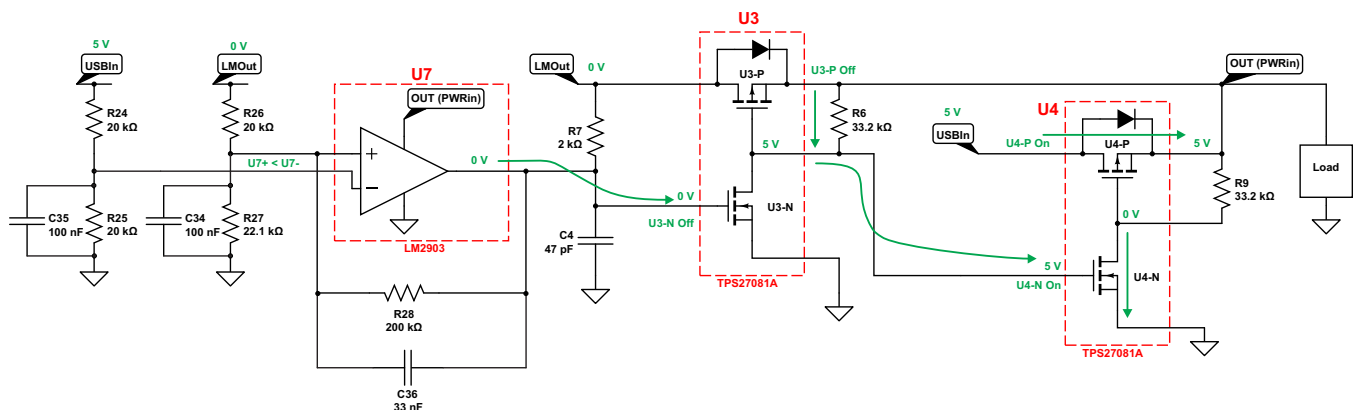
Figure 9. USB Supplied Power ORing

Copyright © 2017, Texas Instruments Incorporated

2.3.3 Comparator Design and Calculations

The comparator's primary function is to provide the system an active method to drive the U3 fets off. When both sources are available, the comparator ensures that the U3 fets will not latch should LMOut become unexpectedly unavailable (that is, 24-V_{AC} power is unplugged). The comparator also prevents a voltage spike due to the drain-to-source capacitance from latching the U3 fets on when USB is initially plugged in. Hysteretics is used on the comparator to ensure the device does not oscillate about the threshold voltage and ensures the U3 fets are turned fully off when switching to USB power.

This section provides the equations necessary to adjust the comparator's input voltage dividers and hysteretics should an adjustment to the default values be desired. The values presented in the following equations reflect the default setup of the TIDA-01395 design. When the comparator output is High-Z, R_{28} is virtually in parallel with R_{26} thus raising the non-inverting terminal of comparator, requiring a higher USB voltage to drive the comparator's output low. The equivalent resistance of R_{26} in parallel with R_{28} is:

$$R_{eqH} = \frac{20 \text{ k}\Omega \times 432 \text{ k}\Omega}{20 \text{ k}\Omega + 432 \text{ k}\Omega} = 19.12 \text{ k}\Omega$$

(12)

Given LMOut is 5 V, the non-inverting input is calculated with a basic voltage divider:

$$IN + LR = LMOut \times \left(\frac{R_{27}}{R_{27} + R_{eqH}} \right) = 5 \text{ V} \times \left(\frac{22.1 \text{ k}\Omega}{22.1 \text{ k}\Omega + 19.12 \text{ k}\Omega} \right) = 2.68 \text{ V}$$

(13)

Therefore, the inverting terminal, must exceed 2.68 V. Because R_{24} and R_{25} are of equal resistance, 20 kΩ, the required USBIn to drive the comparator low is twice the required inverting terminal.

$$USBIn_{LR} = 2 \times IN + LR = 2 \times 2.68 \text{ V} = 5.36 \text{ V}$$

(14)

To account for the opposite scenario, USB was initially present and 24 V_{AC} was subsequently provided, the same threshold calculations must be performed for when the comparator's output was initially low. This scenario is unlikely to occur in the specific end products this TI Design targets; however, such a scenario is planned for regardless.

When the USB is present with LMOut absent, the comparator output is low (see Section 2.3.2). Therefore, R_{28} is virtually in parallel with R_{27} providing an equivalent resistance:

$$R_{eqL} = \frac{22.1 \text{ k}\Omega \times 432 \text{ k}\Omega}{22.1 \text{ k}\Omega + 432 \text{ k}\Omega} = 21.0 \text{ k}\Omega$$

(15)

Given USBIn is at nominal 5 V, and thus the inverting terminal is 2.5 V through the voltage divider of R_{24} and R_{25}, the required LMOut needed to produce a non-inverting terminal voltage greater than 2.5 V is calculated in Equation 16.

$$LMOut_{HZR} = IN - \times \left(\frac{R_{eqL} + R_{26}}{R_{eqL}} \right) = 2.5 \text{ V} \times \left(\frac{21.0 \text{ k}\Omega + 20 \text{ k}\Omega}{21.0 \text{ k}\Omega} \right) = 4.88 \text{ V}$$

(16)

Therefore, 4.88 V is the theoretical voltage LMOut must exceed in order to dominate over a 5.0-V USB input.

2.4 Battery Management

2.4.1 Battery Charging

Battery charging and power path management are performed by the bq24072 in the TIDA-01395. The bq24072 provides a low-cost solution that features independent battery charging and load paths through its power path capability without the need for any external FETs. The device can monitor battery temperature through a dedicated pin, ensures USB compliant inrush current and current limits, and provides PGOOD and charge signals.

The bq24072 is a single-power input device and was specifically chosen over dual-input devices due to cost. The bq24072 and ORing detailed in Section 2.3 provide the same functionality as a fully integrated dual-input device but at a lower cost. The TIDA-01395 is designed with an understanding that end products may have different requirements and that ease of design changes to fit individual systems is necessary. If the end product does not use USB (or a secondary power source in general), the ORing solution and the USB related components detailed in Section 2.2.2 can be eliminated and the single input of the bq24072 can be used for an even lower cost solution. In such a scenario, a dual-input battery management IC would be over-engineered for the application and would incur unnecessary costs or significant design changes. For those reasons, the bq24072 was chosen as the ideal low-cost solution.

The bq24072 features power path capability, allowing the battery to supplement the main power source to meet high load demands. This feature allows the use of a smaller main power source, thus reducing costs further.

Figure 10 displays the setup and components chosen for the TIDA-01395. The bq24072 has a minimum recommended input voltage of 4.35 V, V_{OVP} of 6.6 V, and a maximum absolute input voltage of 28 V. The device charges the battery up to 4.2 V ($V_{BAT(REG)}$). The output is regulated to 200 mV above $V_{BAT(REG)}$.

Copyright © 2016, Texas Instruments Incorporated
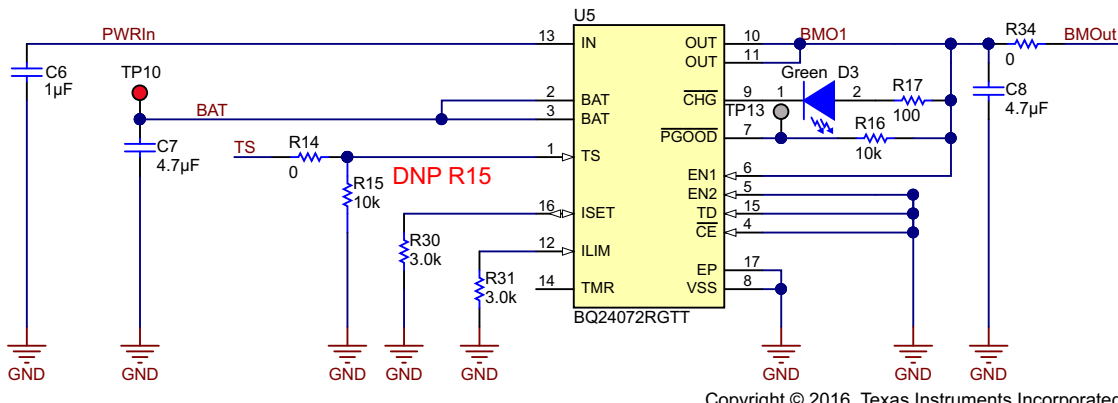
Figure 10. Battery Management Implementation

A small input cap (C6) is chosen as USB 2.0 specifications requires less than 10 μF to be hard started. The bq24072 datasheet recommends between 1 and 10 μF of the input capacitance. A 4.7-μF battery input capacitor (C7) was chosen per datasheet recommendation. The output capacitor (C8) of 4.7 μF is the minimum recommended value per the datasheet.

To comply with USB 2.0 specifications, the input current must be limited to 500 mA. The EN1, EN2, and ILIM pins of the bq24072 allow a programmable current limit. As per datasheet, EN1 is set HIGH and EN2 is set LOW to program a 500-mA current limit. ILIM must not be left floating, as doing so would disable charging, so the ILIM is set to provide a higher current limit (536 mA) than the EN1/EN2 pins, which allows the EN1/EN2 current limit to be the dominant, more conservative limit. Equation 17 shows the calculation used in the TIDA-01395 for R_{31}.

> **NOTE:** K_{ILIM} is a datasheet provided value for current limits above 500 mA.

$$R_{31} = R_{ILIM} = \frac{K_{ILIM}}{I_{IN-MAX}} = \frac{1610 \ A\Omega}{536 \ mA} = 3 \ k\Omega$$

(17)

R_{30} is connected to the ISET pin and determines the battery's fast charge current level ($I_{O(CHG)}$ shown in Figure 11. The calculation for R30 in this TI Design is shown in Equation 18. However, the fast charge current must be chosen depending on the battery specifications used in the end product.

$$R_{30} = R_{ISET} = \frac{K_{ISET}}{I_{O(CHG)}} = \frac{890\ A\Omega}{300\ mA} \cong 3\ k\Omega$$

(18)
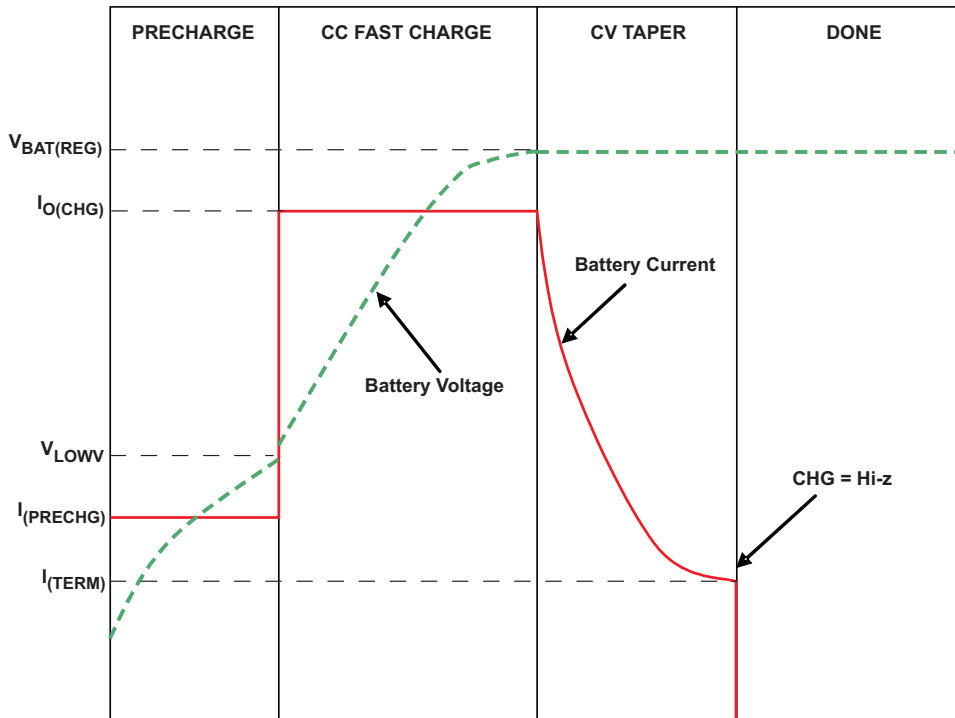
Figure 11. Typical Battery Charge Cycle

Net "TS" is used to monitor the battery temperature on battery packs that have a built-in thermistor. If using TS, R15 must be not populated. Use R15 if leaving TS floating and not using temp sensing. The value of 10k is per datasheet recommendation.

The "TMR" pin is left unconnected to set the pre-charge and fasts-charge safety timers to their default values. The pre-charge safety timer will be set to a typical value of 1800 seconds. The charge safety timer will be set to a typical value of 18000 seconds. Pin "TD" is tied to GND to enable charger termination. Pin "CE" is tied to DNG to enable the battery charger. PGOOD is pulled to VSS when a valid input source is detected and is high impedance when the input power is not within specified limits. PGOOD can sink a maximum of 15 mA so R16 must be chosen appropriately to ensure PGOOD does not sink more than 15 mA.

Pin CHG is pulled to VSS when the battery is charging and is high impedance when the charging is complete or when the charger is disabled. R17 must be chosen to ensure CHG does not sink more than 15 mA. The TIDA-01395 uses an indication LED (D3) on the charge pin. D3 exhibits a typical forward bias voltage of 3.2 V. The appropriate R17 is thus calculated in Equation 19. 100 Ω was chosen to allow less than 15 mA.

$$R_{17} = \frac{V_{OUT(MAX)} - V_{D3(Forward-Bias)}}{15\ mA} = \frac{4.4\ V - 3.2\ V}{15\ mA} = 80\ \Omega$$

(19)
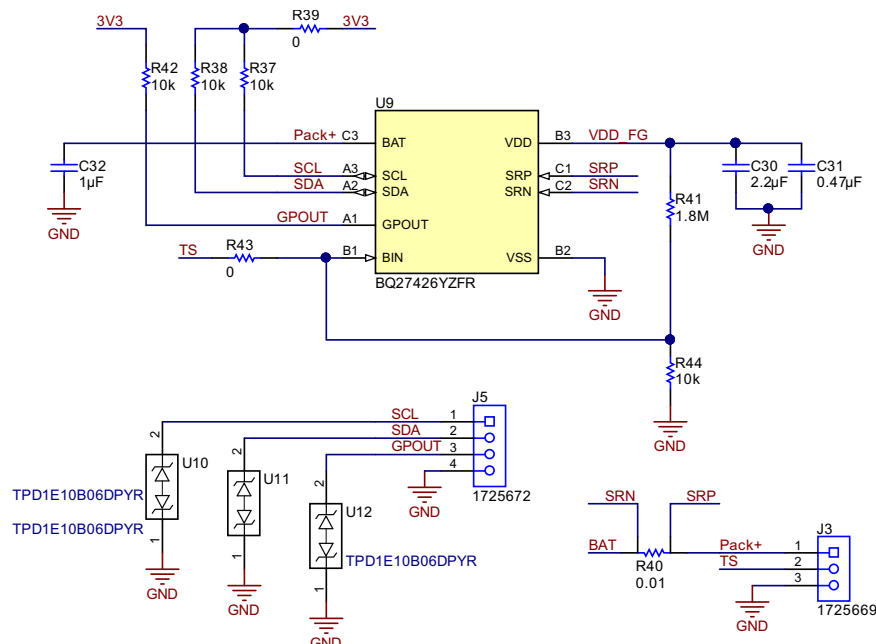
2.4.2 Battery Fuel Gauge

Fuel gauging is performed on the system side by the bq27426 using TI's Impedance Track technology. This device is a low-cost, single-cell fuel gauge that reports remaining capacity, SOC, battery voltage, and estimates the battery's state of health. It is also very accurate due to Texas Instrument's patented Impedance Track technology and adjusts automatically for battery aging, self-discharge, temperature, and rate changes.

Other technologies often require the battery to be fully discharged as often as once a month to maintain fuel gauge accuracy. This is not acceptable in this TI Design because doing so would leave the system without sufficient battery power for a period of time. The Impedance Track functionality used in the bq27426 only requires a discharge to 35% approximately every month. This feature ensures the battery will always have sufficient power in case of a brownout. During system design, it will be important to program an MCU or MPU to allow the battery to discharge to 35% periodically to maintain high accuracy.

The bq27426 is a ROM-based device; therefore, during initial setup or if all power—both main source of power and battery power—is completely lost, reprogramming the device will be necessary. This can be done across the I²C lines. The data needed to be programmed to the fuel gauge upon startup is minimal in size, and all the code necessary is easily exported by Texas Instrument's Battery Management Studio for use in a complete system.

The bq27426 has both an internal temperature sensor and the ability to use an external thermistor. Note that both the bq27426 and the battery charger bq24072 have the ability to use an external thermistor for temperature sensing. However, only one device can use a single thermistor at any given time. Many Li-Ion and Li-Po battery packs may contain a thermistor, and the designer may wish to use this for battery temperature detection. A choice must be made as to which device will be used to detect the temperature of the battery. The bq27426 uses the battery temperature to improve the accuracy of the reported SOC. The TIDA-01395 includes the necessary 0-Ω, pullup, and pulldown resistors to configure the board to use either device for battery temperature measurement. To use the bq27426 for thermistor temperature measurement, R_{44} and R_{14} must be depopulated. If instead the bq24072 is to be connected to the thermistor, R_{43} and R_{15} must be depopulated rather than R_{44} and R_{14}. The TIDA-01395 board is initially configured to use the bq27426 for battery temperature measurement.

Copyright © 2017, Texas Instruments Incorporated

Figure 12. Battery Fuel Gauge Schematic
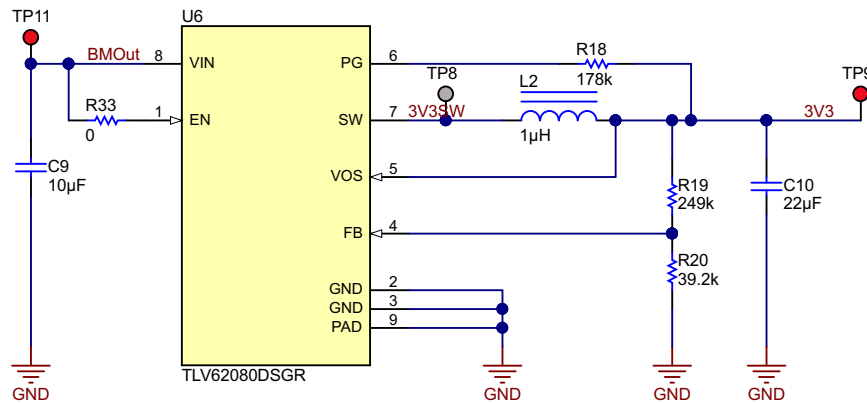
As shown in Figure 12, C_{30}, C_{31}, and C_{32} were chosen per the bq27427 datasheet as 2.2 µF, 0.47 µF, and 1 µF, respectively[12]. R_{37}, R_{38}, and R_{42} serve as pullup resistors for the communication lines. U10, U11, and U12 serve as ESD protection for those same communication lines. As per datasheet, pin "BIN" must not be left floating, so R_{41} is used to provide a pullup to net "VDD_FG" for the "BIN" pin in case the battery is removed. Pin VDD is an internal LDO and must not be used to power any external load.

R_{40} is a 10-mΩ sense resistor to allow the fuel gauge to perform coulomb counting. The TIDA-01395 uses a four-pin sense resistor for ease of layout and accuracy. If a standard two-pin sense resistor is used, take additional care during layout to maintain high-accuracy and low-noise performance. Pins "SRP" and "SRN" are the sensing pins to be connected to either side of the sense resistor with "SRP" on the positive battery terminal side of the resistor and "SRN" on the other.

2.5　*3.3-V Rail—TLV62080*

The 3.3-V rail serves as the main power output that directly supplies power to the various system components in the end product. The input of the TLV62080 is connected to the output of the bq24072. The 3.3-V rail ultimately receives its power from either the 24-V_{AC} line, USB, or the battery, depending on which source is available. Devices powered from this rail are battery backup protected and benefit from the power assistance features of the bq24072.

The TLV62080 is a very lost cost, low BOM count, high efficient step-down converter. It has a 100% duty cycle capability, which is particularly useful in battery powered applications such as the TIDA-01395 to achieve the longest operation time by taking full advantage of the whole battery voltage range. The converter features DCS-Control (direct control with seamless transition into power save mode) architecture to achieve excellent load transient performance and output voltage regulation accuracy. The TLV62080 as an output current max of 1.2 A. Should more than a 1.2-A output be required, the TLV62084 offers pin-to-pin compatibility (though the input and output capacitors as well as inductor may need to be changed appropriately) with the TLV62080 but features a 2-A output current. Figure 13 shows the specific system implementation in the TIDA-01395 and highlights the simplicity of the part and the low external BOM count.

Copyright © 2016, Texas Instruments Incorporated

Figure 13. TLV62080 Implementation

Proper inductor selection is critical for buck converters, particularly the inductor value and the saturation current of the inductor. To calculate the maximum inductor current under static load conditions Equation 20 and Equation 21 are used. $I_{OUT,MAX}$ is 1 A per TIDA-01395 specifications. A desired ΔI_L of approximately 40% of $I_{OUT,MAX}$ is used to set ΔI_L to 0.4 A. During medium to heavy load conditions, the TLV62080 operates in PWM mode at a nominal switching frequency (f_{SW}) of 2 MHz. A maximum input voltage of 4.4 V is used as specified in Section 2.4.

$$I_{L,MAX} = I_{OUT,MAX} + \frac{\Delta I_L}{2} = 1A + \frac{0.4\,A}{2} = 1.2\,A \tag{20}$$

$$L = V_{OUT} \times \left(\frac{1 - \dfrac{V_{OUT}}{V_{IN}}}{F_{SW} \times \Delta I_L} \right) = 3.3\,V \times \left(\frac{1 - \dfrac{3.3\,V}{4.4\,V}}{2\,MHz \times 0.4} \right) = 1.03\,\mu H \cong 1\,\mu H \tag{21}$$

As calculated in Equation 20 and Equation 21, a 1-µH inductor must be chosen. Standard practice is to choose an inductor with a saturation current at least 20% to 30% percent higher than $I_{L,MAX}$. The XFL3012-102ME Inductor by manufacturer Coilcraft is a 1-µH inductor with a 2500-mA current rating, a low DC resistance of 35 mΩ, is recommended by the TLV62080 datasheet, and was chosen for L2 in the TIDA-01395.

The output capacitor (C10) value of 22 µF was chosen based on the TLV62080 datasheet recommended output capacitor and inductor combinations. The recommended capacitance anticipates capacitance tolerance and bias voltage de-rating. The effective capacitance can vary by 20% and –50%. An input capacitance (C9) of 10 µF was chosen per datasheet recommendation and will be sufficient for most applications, a larger value reduces input current ripple.

For best accuracy, R_{20} must be kept smaller than 40 kΩ to ensure that the current flowing through R_{20} is at least 100 times larger than I_{FB}. Using Equation 22, a desired output voltage of 3.3 V, a datasheet specified feedback regulation voltage of 0.45 V, and a chosen R_{20} value of 39.2 kΩ, R_{19} is calculated to be 249 kΩ. As with most applications, tight tolerance resistors (less than or equal to 1%) should be used for the feedback network.

$$V_{OUT} = V_{FB} \times \left(1 + \frac{R_{19}}{R_{20}} \right) = 0.45 \text{ V} \times \left(1 + \frac{249 \text{ k}\Omega}{39.2 \text{ k}\Omega} \right) = 3.3 \text{ V}$$

(22)

VOS serves as the output voltage sense terminal for the internal control loop and must be connected to the output.

3   Getting Started Software and Hardware

3.1   Hardware

Several test points are made available for the each process on the PCB. However, when performing ripple, transient, and efficiency tests, the break out test points should not be used due to parasitic noise. Instead, the output, input, or other point of interest should be measured as close to the IC pins as possible.

Examples of transient test setups are shown in Figure 14, Figure 15, and Figure 16 that uses a barrel wire to GND technique and the current carrying wires soldered directly onto the output capacitor of the DC-DC being tested. These current carrying wires are connected directly to a programmable electronic load and the current is measured through a current probe. When performing efficiency plots, separate wires from the current carrying wires must be used, as shown in Figure 17 to avoid inaccurate measurements due to line voltage drops.
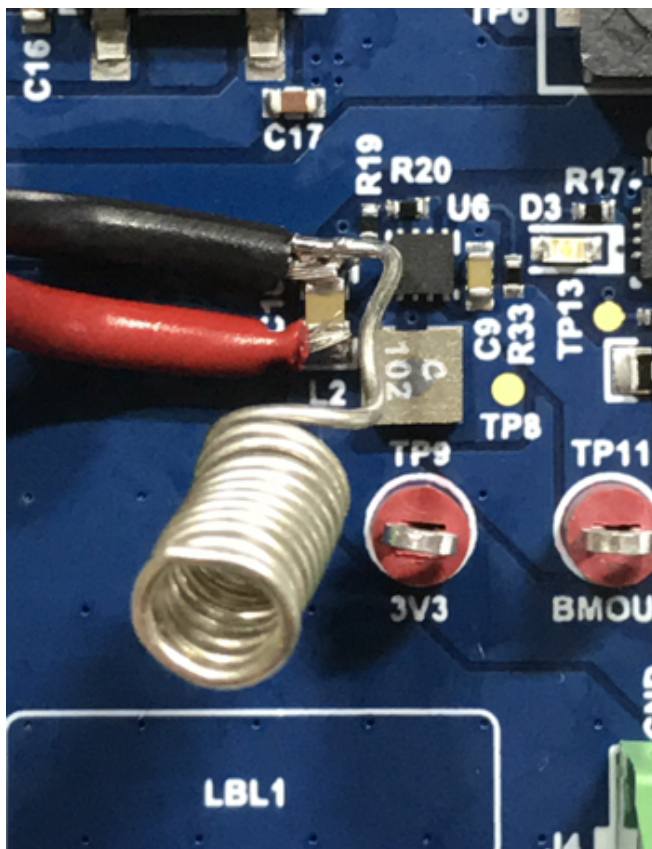
Figure 14. Soldered Output Wires Test Setup   **Figure 15. Scope Probe and Barrel Test Setup**
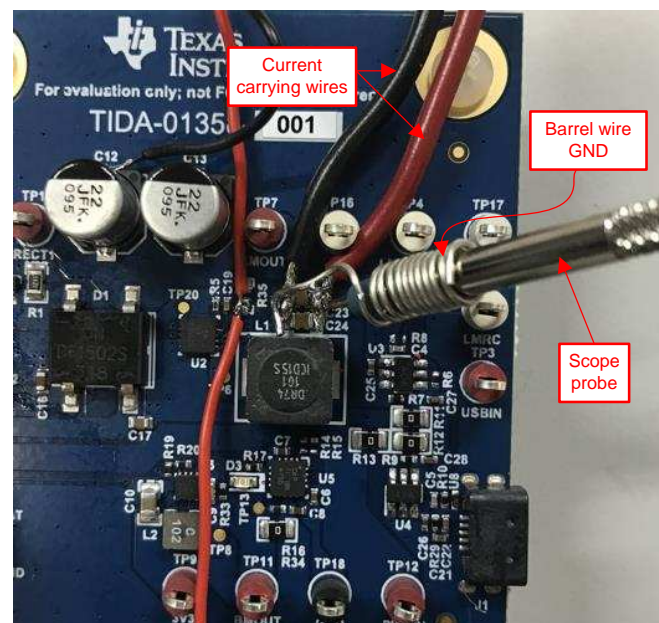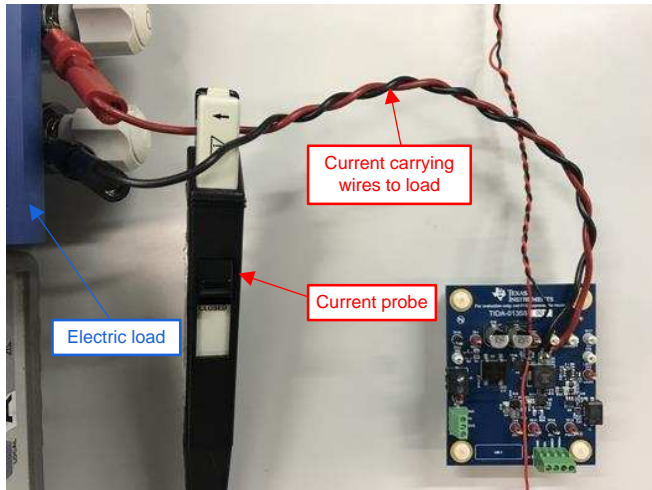
Figure 16. Current Probe and Electronic Load Test Setup
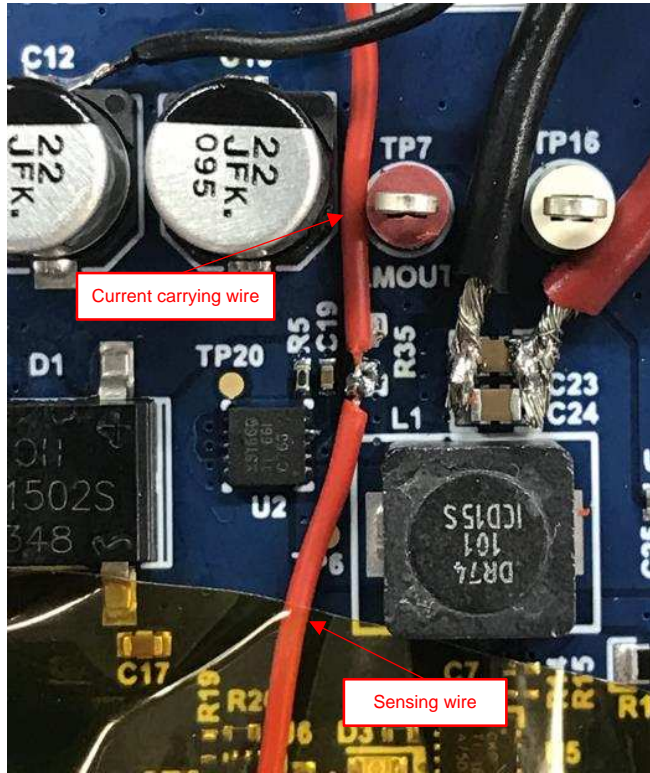
Figure 17. Separate Sensing and Current Carrying Wires Test Setup

3.2   Software

During the design phase, characterizing the battery to be used is necessary for the best fuel gauge performance. The manual portion of this process only needs to be done once, and Texas Instruments provides several tools and resources that allow this process to be done easily, allowing quick system bring-up.

The primary software that will be used for characterization and testing is Battery Management Studio (bqStudio). The EV2400 or the Gauge Development Kit (GDK) can be used to interface between bqStudio and the bq27426 fuel gauge. The TIDA-01395 provides all the necessary pinouts through J5 (as shown in Figure 12) to connect to either of these devices.

The bq27426 has three selectable pre-programmed profiles. The first step in characterizing the battery is to determine which of these three profiles best matches the battery characteristics. Note that it may be the case a 4.2-V battery is best characterized for most of its discharge curve by the 4.35-V profile, as was the case for the battery arbitrarily chosen for testing this TI Design and design guide. To do so, TI provides a Gauging Parameter Calculator. The technical reference document *Simple Guide to Chemical ID Selection Tool (GPC)* provides a five-page, easy-to-read guide on how to log the charge and discharge curve with bqStudio and how to submit it to the GPC tool.

To provide a quick overview in this design guide, GDK is used. The GDK is connect to the TIDA-01395 using the I^{2}C terminals and the EXT_Load– and EXT_Load+ connect to GND and BMOut, respectively. With bqStudio open and communicating with the fuel gauge, ensure the "Registers" tab and the "GDK" tab are available. It is best to have the battery at least partially discharged before proceeding. Open the "Registers" tab, click "Start Log", and save it to an appropriate location. Open the "GDK" tab and open the "Auto Cycle" sub-tab as shown in Figure 18. The device must relax for 120 minutes after charge and 300 minutes after discharge. The other parameters may be adjusted depending on the specific battery being used. For the lithium polymer battery used, 3000 mV is a standard termination voltage. Once the parameters are set, click the "Start" button and wait for the cycles to complete.
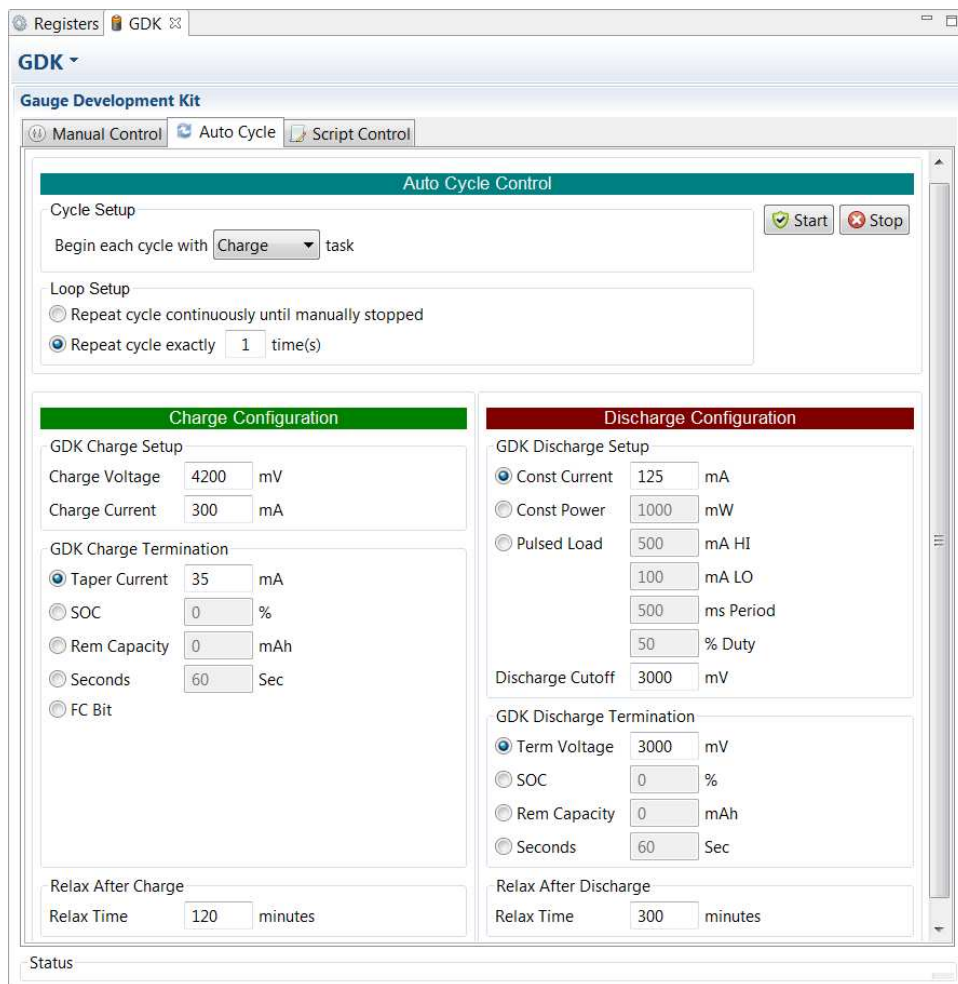
Figure 18. GDK Setup for Initial Discharge Testing

Once the cycle has completed, including the relax time, stop logging. The GPC tool requires a single .zip file containing one configuration file, or one data file, as input. The name of the .zip file is not important. The .zip file should contain the following files:

- config.txt
- roomtemp_rel_dis_rel.csv

roomtemp_rel_dis_rel.csv is derived from the log file. Open the log file in Excel®, and delete all top rows that are not data, taking note of which columns are the "Voltage", "Current", "ElapsedTime", and "Temperature" because this information is needed for the config.txt file. Save this as a .csv file.

The configuration file is a text file named config.txt and is an ASCII text dictionary containing the following information:

- Processing Type = 2; determines the type of tool used. The value should be 2 for the chemistry ID selection tool
- NumCellSeries = Number of series cells
- VoltageColumn = Zero-based column number for the voltage data in the .csv data log
- CurrentColumn = Zero-based column number for the current data in the .csv data log
- TemperatureColumn = Zero-based column number for the temperature data in the .csv data log
- ElapsedTimeColumn = Zero-based column number for the elapsed time data in the .csv data log

Copyright © 2017, Texas Instruments Incorporated

Once the .zip file is submitted to the online GPC calculator, the user will receive an email containing a .zip file of the battery testing report. That .zip file contains the GPC_report.txt file, which reports the predicted max DOD error % for all available profiles based on the log data. Towards the bottom of the text file, the bq27426 will show the three pre-programmed profiles in order of least DOD error to most. The following example results show the report for the battery used for testing in this TI Design. The report identifies the best generic ID to be 3230 with a max DOD error of 13.64%. While this max error appears extremely high, it is only the predicted error before any learning cycles. Once a learning cycle has been performed, the impedance tables and Qmax will be updated appropriately and error will decrease significantly. In this design guide, for example, the error was reduced to less than 2% after a single learning cycle.

```
Device / Family #3
Generic Chem ID    Device/ Voltage/ Chemistry    max DOD error, %
3230    bq27426: (default) 4.35V LiCoO2    13.64
3142    bq27426: (ALT-CHEM2) 4.4V LiCoO2    14.72
1202    bq27426: (ALT_CHEM1) 4.2V LiCoO2    23.87
Best generic ID 3230
```

The best generic ID can then be programmed into the fuel gauge from the "Chemistry" tab in bqStudio.

Before performing the learning cycle, a few basic parameters must be set based on the battery being used. These parameters are located in the sub-menus of the "Data Memory" tab in bqStudio:

- Design Capacity
- Design Energy
- Terminate Voltage
- Taper Rate (Note that the Unit is .1 Hr rate)
- V at Chg Term
- Taper Voltage
- Dsg Current Threshold (the current threshold when the fuel gauge goes into sleep mode during discharge)
- Chg Current Threshold (the current threshold when the fuel gauge goes into sleep mode during discharge)

The following values are used in the TIDA-01395:

- Design Capacity = 1250 mAh
- Design Energy = 4600 mWh
- Terminate Voltage = 3350 mV
- Taper Rate = 250 .1 Hr rate
- V at Chg Term = 4200 mV
- Taper Voltage = 4100 mV
- Dsg Current Threshold = 650 .1 Hr rate
- Chg Current Threshold = 100 .1 Hr rate

The next step is to perform an initial learning cycle that will allow the gauge to update the maximum capacity of the battery ("Qmax Cell 0") as well as the impedance table. The application report *Achieving The Successful Learning Cycle* is a quick four-page guide on how the gauge performs the learning cycle and what to expect. It is recommended to use the EV2400 or GDK during this initial learning cycle for logging and testing purposes. However, the gauge is actually performing the learning cycle and will independently continue to update its impedance table and Qmax as the battery ages during the life of the system. The GDK can be used to automate the charging and discharging phases by acting like an electronic load; however, a normal electronic load and the battery charger on the TIDA-01395 board can also be used. For the tests shown in this design guide, the learning cycle was performed with a 300-mA charge and a 125-mA (C/10) discharge rate using the GDK.

To perform the initial learning cycle, the battery must be fully discharged and relaxed. A similar setup to Figure 18 is used but with the "Discharge Cutoff" and "Term Voltage" set to 3350 mV. 3350 mV is chosen in the TIDA-01395 because the TLV62080 outputs 3.3 V and thus needs an input greater than 3.3 V to properly operate. Therefore, when the battery reaches 3350 mV, the fuel gauge will show a 0% SOC in this TI Design. Note the gauge has to detect that the cell has a full charge when the charger terminates, so the proper "V at Chg Term" and "Taper Rate" must be set appropriately. Once the learning cycle is complete, the Qmax Cell 0 and the Impedance and RA tables will update.

Finally, an image of the configuration can be saved to be later imported or programmed to other devices. This save is done in bqStudio by clicking on the "Golden Image" Tab and exporting a GMFS file. The GMFS file can later be imported under the "Data Memory" tab, and all parameters will be loaded and programmed to the fuel gauge.

4   Testing and Results

This section details the several tests performed on the TIDA-01395. When testing ripple, transients, and efficiency, the point of measurement is crucial to get accurate measurements. See Section 3 for more testing details.

4.1   Startup, Shutdown, and ORing

This section analyzes the 24-V_{AC} system startup, its soft-start functionality, and provides data showing the consecutive power up of each power stage. USB power is also tested covering the USB specifications voltage range. ORing between the 24-V_{AC} and USB systems are also tested and detailed.

4.1.1   24-V_{AC} Startup and Shutdown

Figure 19 shows the sequence of power up when a 24-V_{AC} system is plugged in. The battery was already connected and powering the 3V3 rail before 24 V_{AC} was plugged in. Upon the 24-V_{AC} plugin, the system begins charging the battery and takes over powering the system load. RectOut reaches steady state in approximately 300 ms from the initial 24-V_{AC} plugin. Variances in the 24-V_{AC} transformer will cause variances in the steady-state rise time as can be seen by comparing Figure 19, Figure 23 and Figure 25. The LM5166 rail (PWRIn) will however power up before steady state is reach as the LM5166 only requires greater than 5 V to be present. Note that the LM5166 rail is tested at node PWRIn, which is directly on the output of the ORing solution. The 3V3 rail exhibits no distinguishable transient response during the transition from battery power to 24-V_{AC} power. Figure 23 and Figure 25 provide startup tests to account for tolerances present in 24-V_{AC} transformers and show comparable results to Figure 19.

Immediate loss of 24-V_{AC} power is tested in Figure 20, Figure 24, and Figure 26. As is evident by the smooth nature of RectOut in these tests, the battery was fully charged and no significant load current was being supplied. Upon a 24-V_{AC} power loss, RectOut discharges most of the rectification caps energy in 1 second for a nominal 24 V_{AC}.

Figure 21 and Figure 22 show a 24-V_{AC} loss while a load on the 3V3 bus is demanding current. The rectification caps discharge considerably faster than no load conditions. The BMOut rail drops in voltage as the BM24072 parts transitions to battery power. The 3V3 rail exhibits no significant transient response to the loss of 24 V_{AC} and remains regulated and supplying to output load.
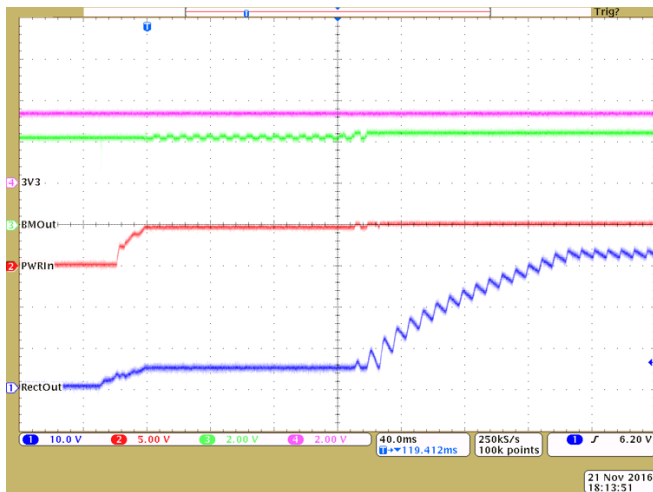
Figure 19. 24-V_{AC} Startup
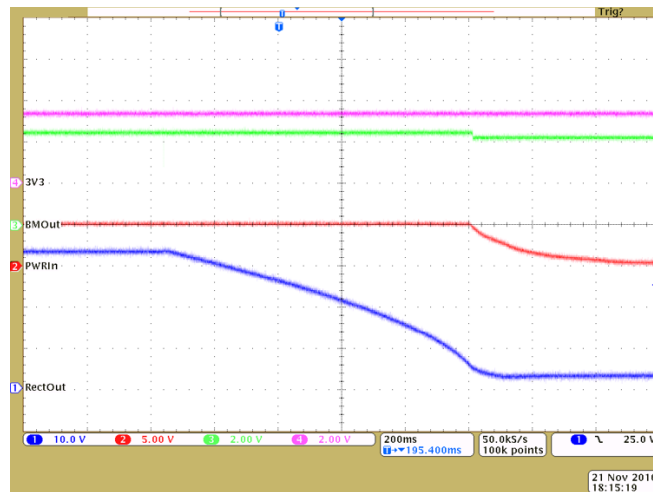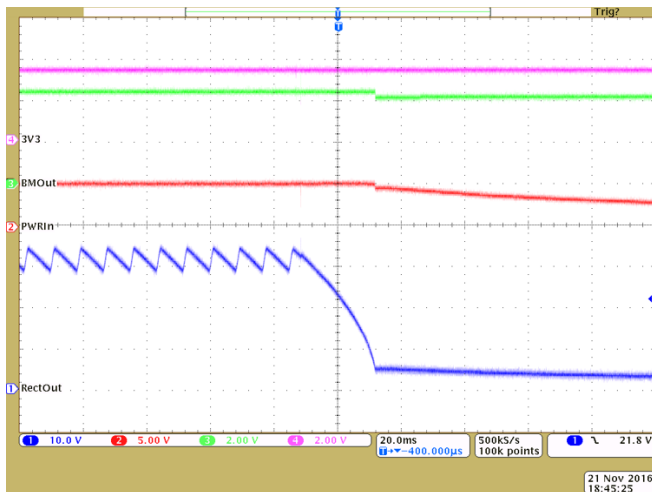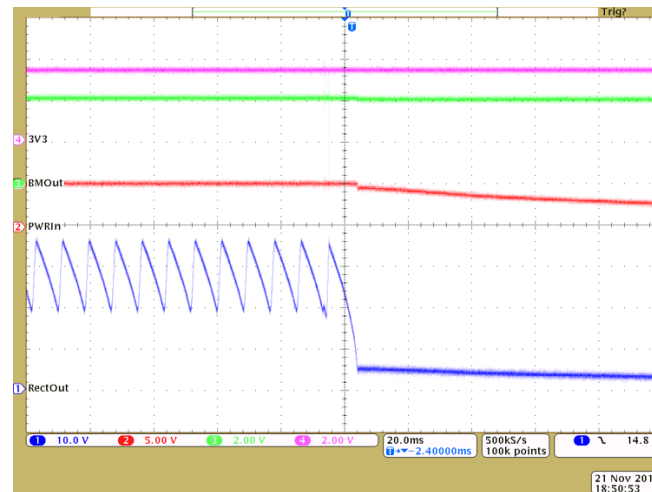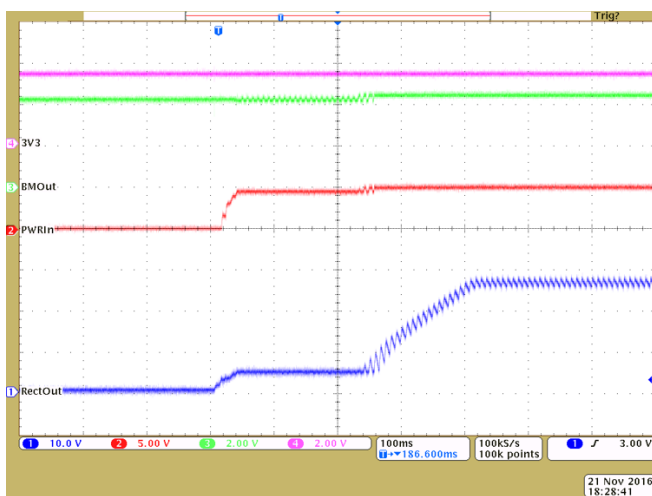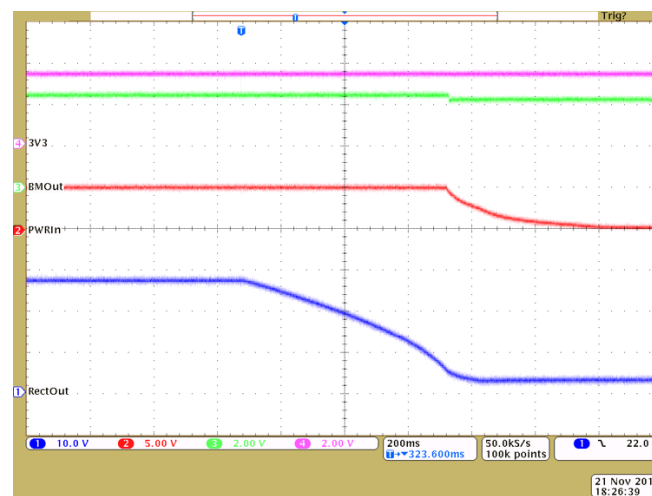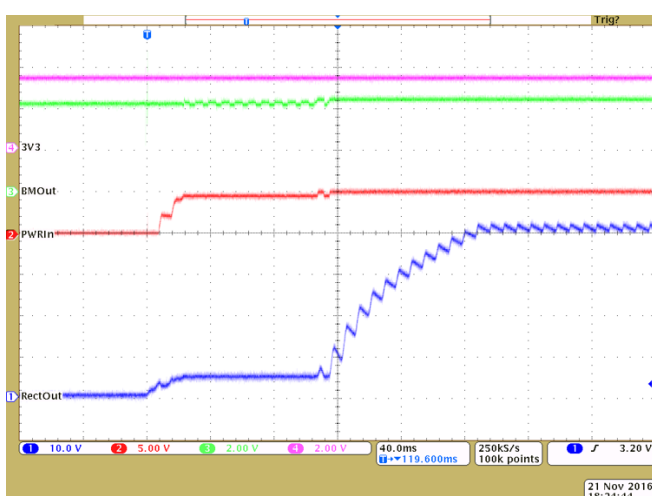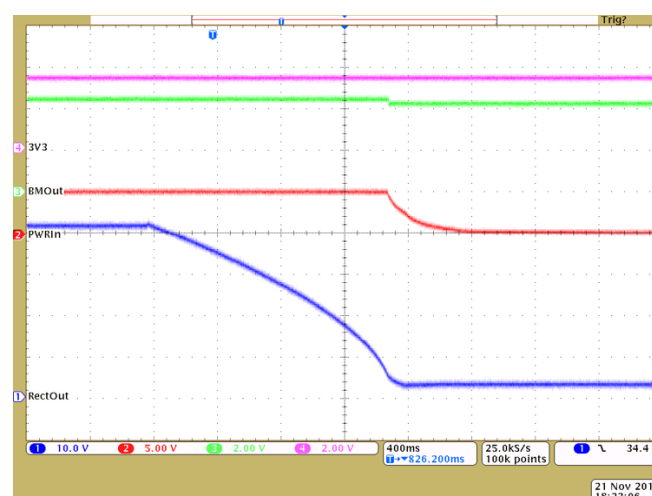
Figure 20. 24-V_{AC} Shutdown

Figure 21. 24-V$_{AC}$ Shutdown (3V3 Load = 200 mA)

Figure 22. 24-V$_{AC}$ Shutdown (3V3 Load = 750 mA)

Figure 23. 20-V$_{AC}$ Startup

Figure 24. 20-V$_{AC}$ Shutdown

Figure 25. 30-V$_{AC}$ Startup

Figure 26. 30-V$_{AC}$ Shutdown

4.1.2 USB Startup and Shutdown

Figure 27 shows a 5.1-V USB cable being plugged into the system (Note: A 3-ft USB A to USB micro-B cable was used for Figure 27 and Figure 28). The node USBin exhibits no overshoot, which is due, in part, to the snubber circuit detailed in Section 2.2.2. The PWRIn, which is the output of the ORing circuit, matches the response of the USBin. This test shows 1.85 ms passes before the battery management system regulates the output, BMOut, to 200 mV plus V_{BATT}. As with the 24-V_{AC} startup, the battery was previously supplying the load when the USB was plugged in. Upon USB plugin, the battery management will begin charging the battery with up to 300 mA. The 3V3 rail show no significant transient response to the change in power sources.

Figure 28 shows power transition back to the battery as the USB is unplugged. Approximately 100 ms passes before the USBIn rail diminishes towards zero. A slight drop at BMOut can bee seen as the system switches to battery power and thus V_{BATT}. The 3V3 rail remains very steady with no significant transient response during the transition.
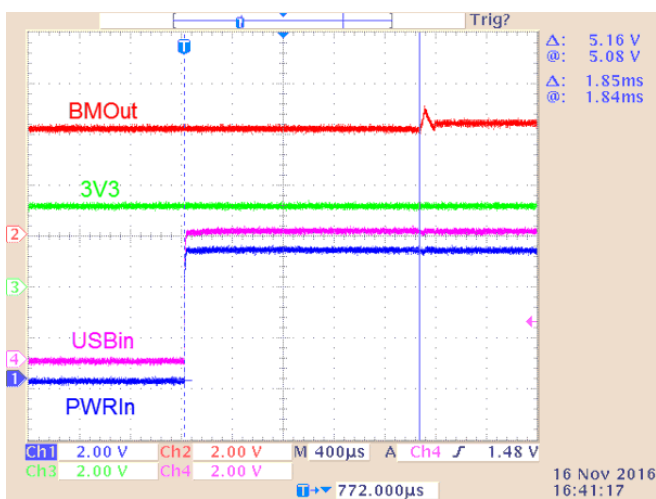
Figure 27. USB 5.1-V Startup
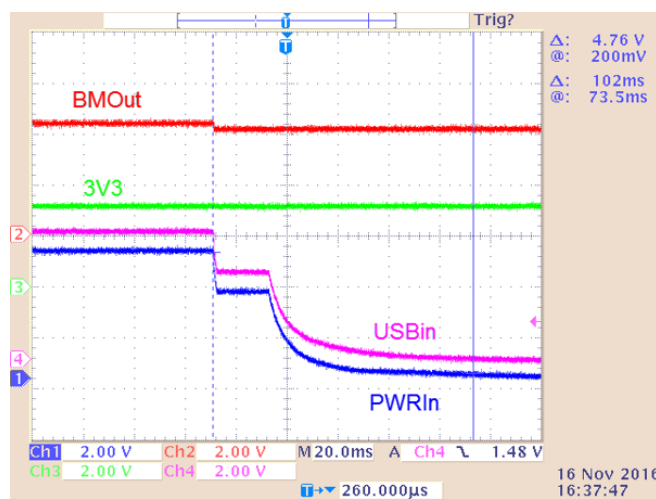
Figure 28. USB 5.1-V Shutdown

Figure 29 shows a startup variation with USBin at 4.35 V, the minimum allowed per USB 2.0 specifications. The actual tests for Figure 29 through Figure 30 were performed with banana to grabber cables. These cables are not isolated and exhibit significantly more parasitic inductance than a typical USB cable. Even so, a very minimal overshoot of 160 mV is observed. The high level voltage of the USB rail is reached approximately 2 µs after initial plugin. As observed in Figure 29, the delay time for the ORing circuit to pass the USBin to the PWRIn rail is approximately 1 µs. Figure 31 and Figure 32 show similar results.
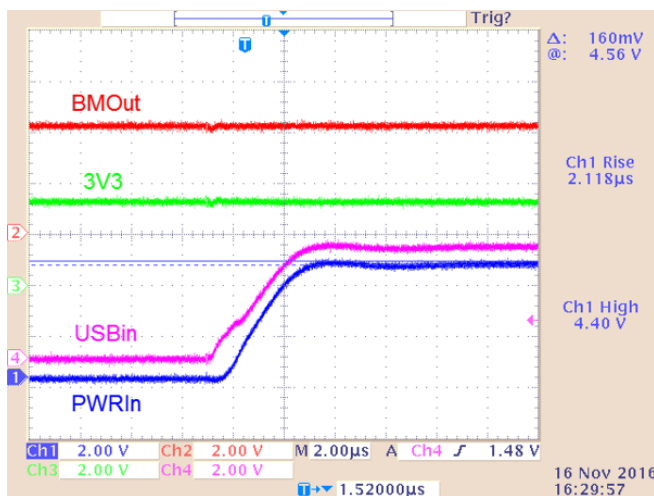
Figure 29. USB 4.35-V Startup
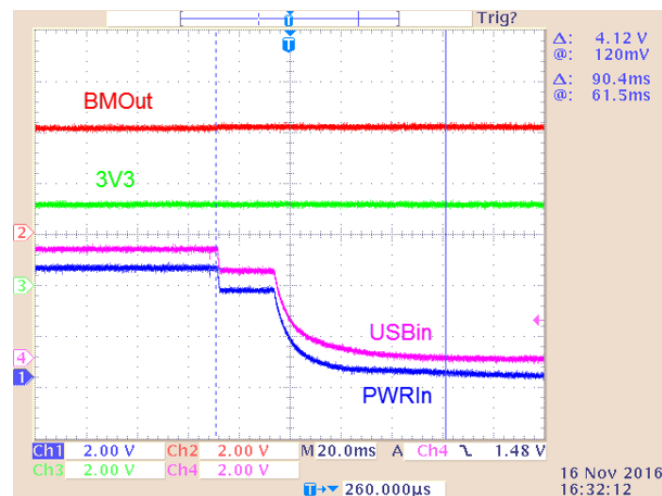
Figure 30. USB 4.35-V Shutdown
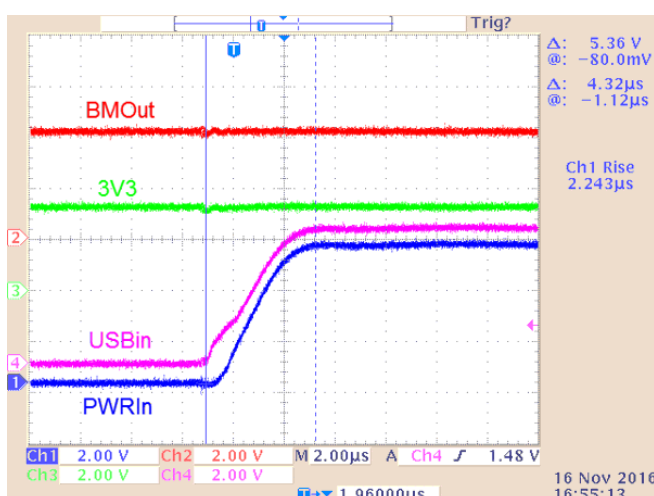
Figure 31. USB 5.25-V Startup
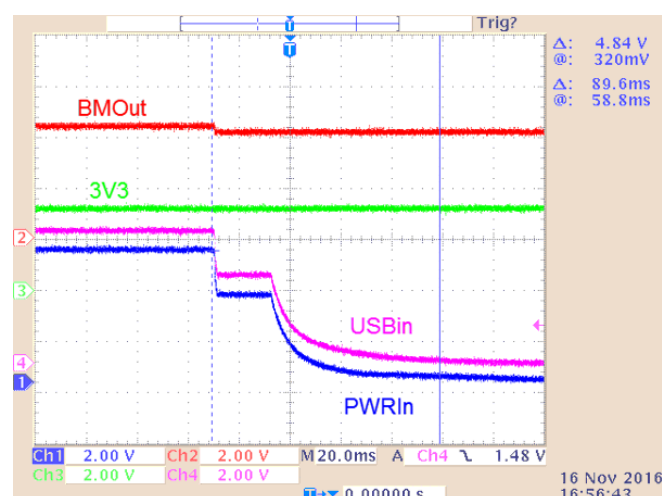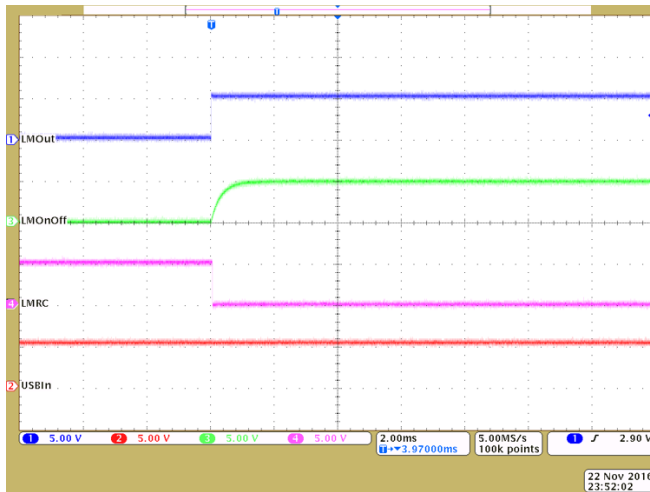
Figure 32. USB 5.25-V Shutdown

4.1.3   ORing
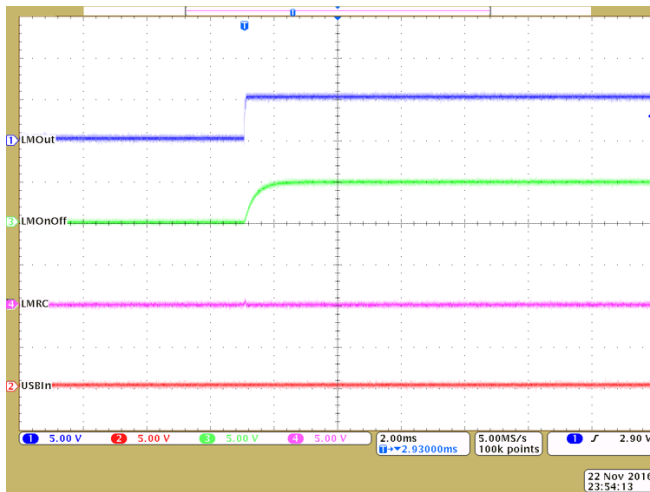
The ORing circuit as described in Section 2.3 is tested in this section. Figure 33 shows LMOut dominating USB upon plugin. Prior to LMOut powering up, USB is shown high and LMRC is high, forcing the USBin associated fets on and LMOut fets off. Once LMOut is powered up, the LMOnOff node begins to be pulled up, thus driving LMRC low, thereby turning the LM associated FETs on, and the USB associated FETs off. Figure 34 shows the opposite activity when LMOut shifts low. When the USB power is not present, LMOut still passes through to output by pulling LMOnOff high as shown in Figure 35 and Figure 36.
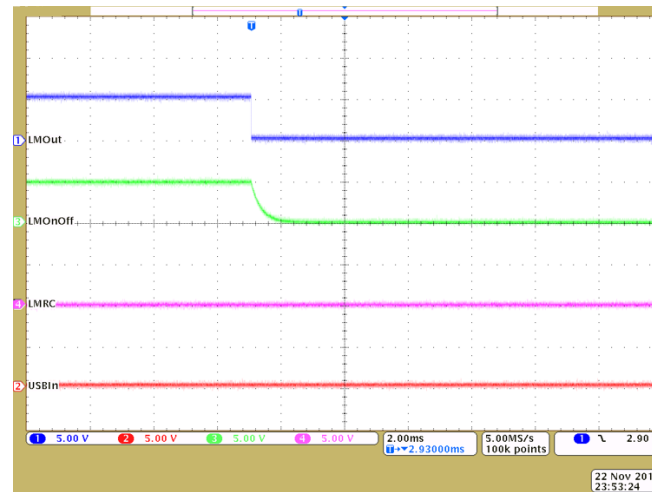
Figure 33. ORing Startup (LMOut Power Up;
USB Source Present)

Figure 34. ORing Shutdown (LMOut Power Loss;
USB Source Present)

Figure 35. ORing Startup (LMOut Power Up;
USB Source Absent)

Figure 36. ORing Shutdown (LMOut Power Loss;
USB Source Absent)

4.2 Load Transients

This section provides load transient data for each of the main DC power stages (LM5166, bq24072, and TLV62080). A summary of transient measurements for switching regulators are provide in Table 2.

Table 2. Load Transient Test Data Summary

DEVICE	NODE NAME	LOAD STEP (mA)	TRANSIENT AMPLITUDE (mV)	TRANSIENT PERCENTAGE	TEST DATA FIGURE
LM5166	LMOut	0 to 480	236.0	4.72%	Figure 37
		200 to 480	104.0	2.08%	Figure 38
TLV62080	3V3	250 to 750	34.5	1.05%	Figure 40
		0 to 1000	61.1	1.85%	Figure 41

4.2.1 LM5166

Figure 37 shows the transition of the LM5166 from DCM to CCM operating modes as is evident by the differing ripple frequencies during no load and 480 mA. A transition from DCM to CCM will cause the worst case transient response. The transient response while operating only in CCM is significantly smaller as seen in Figure 38. Figure 39 provides the load current rise and associated transient response on a small time scale to allow closer analysis.
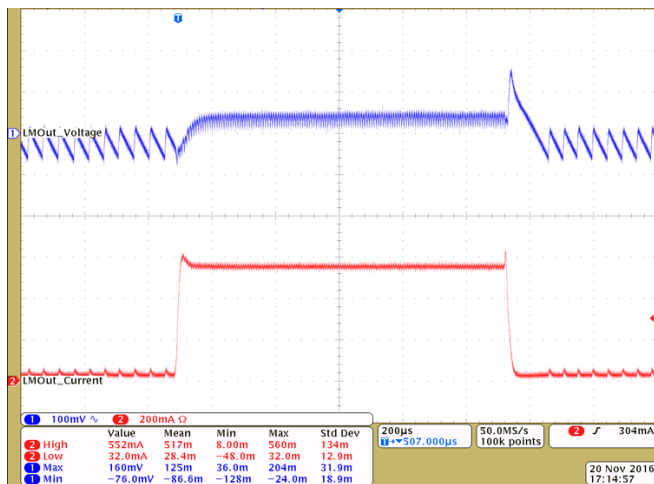
Figure 37. LM5166 Transient Response (0 to 480 mA)
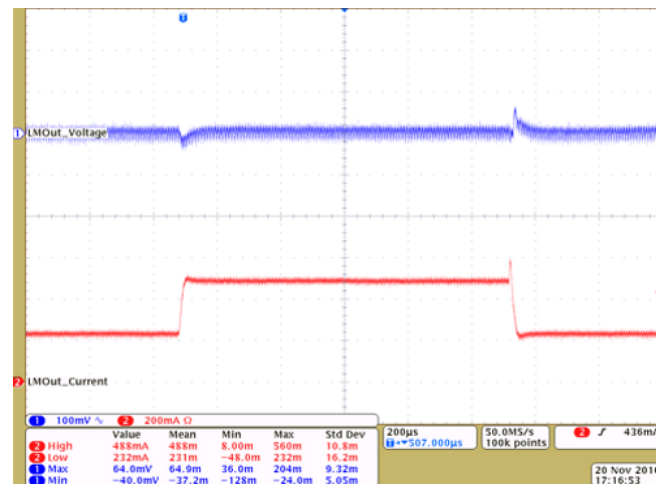
Figure 38. LM5166 Transient Response (200 to 480 mA)
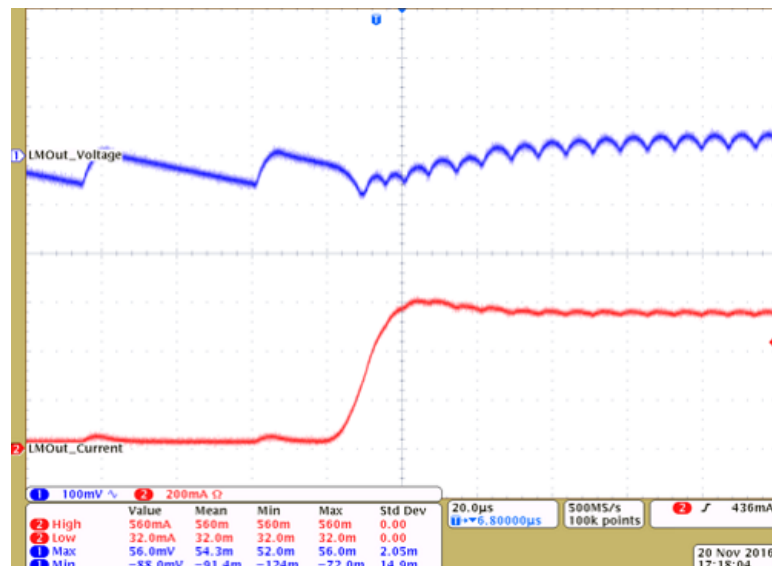
Figure 39. LM5166 Transient Response Slew

4.2.2   TLV62080 Transient Response

The 3V3 rail will be the primary power bus powering a system load and thus ripple and transient response on this rail must remain small. In this TI Design, the TLV62080 operates very well, with a transient response of less than 2% for a 0- to 1-A load step.
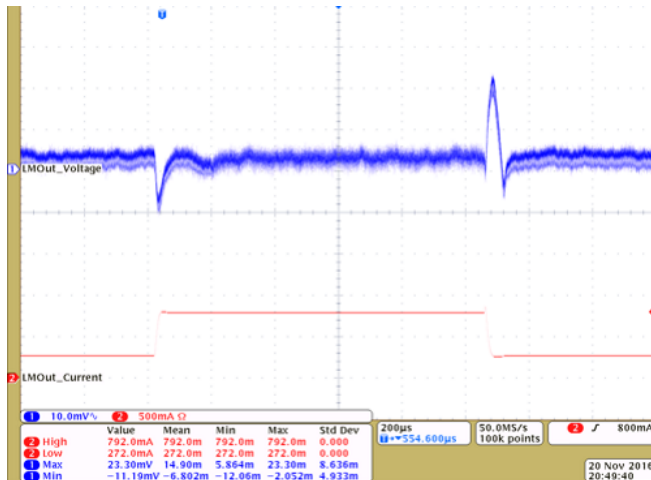
Figure 40. TLV61080 Transient Response (250 to 750 mA)
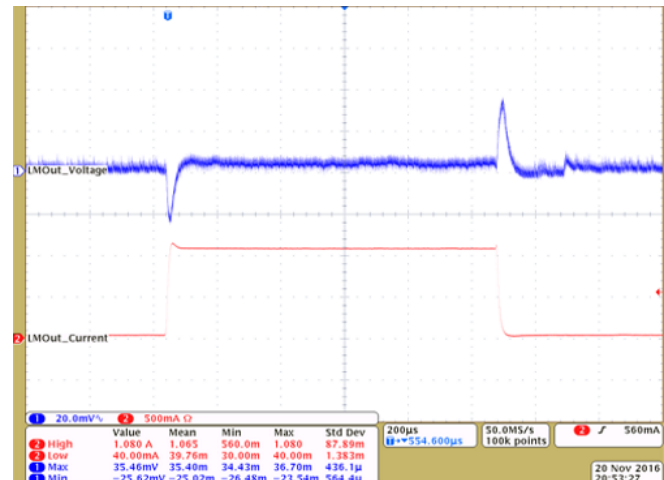
Figure 41. TLV62080 Transient Response (0 to 1 A)
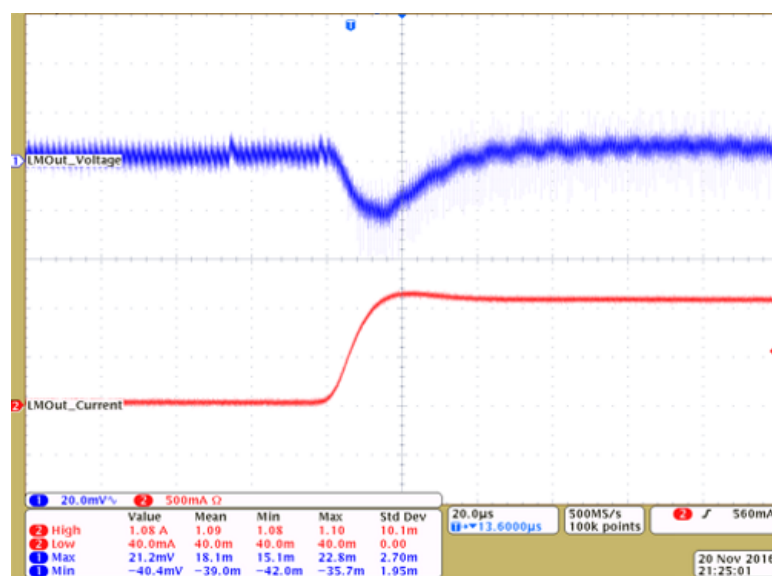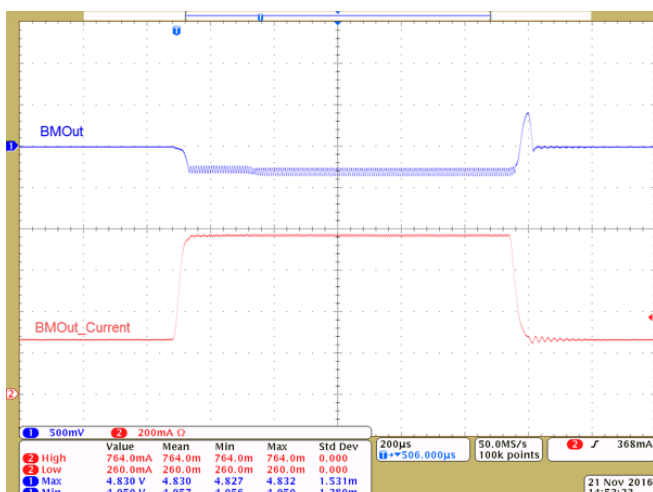
Figure 42. TLV62080 Transient Response Slew
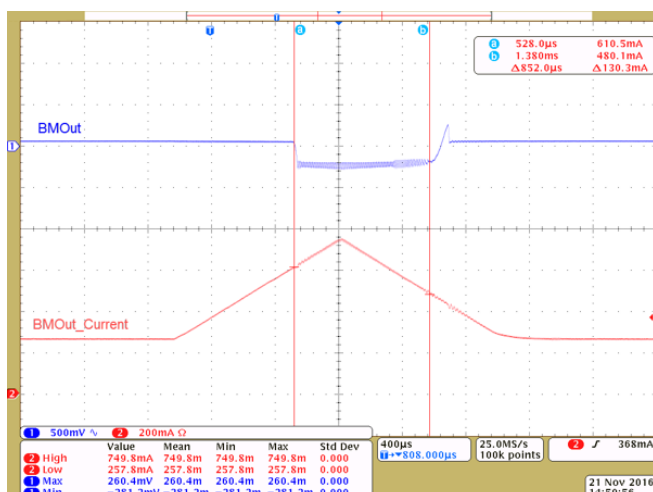
4.2.3 BM24072 Transient Response

The battery management system transient response is more complicated than the LM5266 and TLV62080 as the BM24072 must pull current from two sources, the battery and the PWRin node, when load currents exceed 500 mA. Figure 43 shows a 250- to 750-mA load step on the BM24072 output. As the load current becomes too high for the PWRin node to supply, the battery management system drops in voltage as it uses the battery as power assistance. BMOut returns to the initial voltage once the output current steps back down and the battery is no longer required to provide additional current. Figure 44 shows the battery management power assist beginning when the load current crosses above 610 mA and ceasing when crossing below 480 mA. However, the BMOut voltage, which is dependant on the battery voltage, will change those crossover points. A lower BMOut voltage will raise the current crossover point at which battery power assistance is needed.

When the battery is the only source present, the transient response of the BM24072 exhibits only the voltage drop across the battery's power line as current is pulled as shown in Figure 45.

**Figure 43. BM24072 Transient Response
(250- to 750-mA; Battery and PWRin Source)**

**Figure 44. BMOut Transient Response
(250- to 750-mA Slow Ramp; Battery and PWRin Source)**
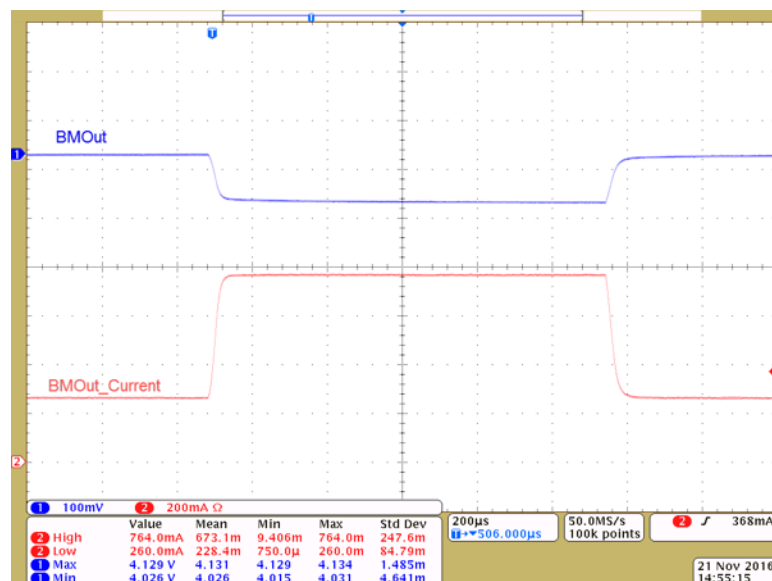
Figure 45. BM24702 Transient Response (250 to 750 mA; Battery Only)

4.3   *Output Ripple*

The output ripple is measured at full load and light load for all three DC stages (LM5166, bq24072, TLV62080). For the LM5166 and the TLV62080, additional measurements are taken to observe the difference in ripple during DCM and CCM operation.

Table 3. Output Ripple Test Summary

DEVICE	NODE NAME	LOAD	RIPPLE AMPLITUDE (mV)	RIPPLE PERCENTAGE	TEST DATA FIGURE
TLV62080	3V3	0 (DCM operation)	14.0	0.42%	Figure 46
	3V3	90 mA (DCM operation)	13.2	0.40%	Figure 47
	3V3	125 mA (CCM operation)	11.9	0.36%	Figure 48
	3V3	1 A (CCM operation)	23.9	0.72%	Figure 50
LM5166	LMOut	0 (DCM operation)	98.0	1.96%	Figure 53
	LMOut	130 mA (DCM operation)	100.0	2.00%	Figure 54
	LMOut	180 mA (CCM operation)	47.0	0.94%	Figure 55
	LMOut	490 mA (CCM operation)	45.4	0.91%	Figure 57
BM24072	BMOut	0 A	5.5	0.14% (V_{BMOut}=4.0V)	Figure 58
	BMOut	500 mA (Battery and USB source)	88.4	2.2% (V_{BMOut}=4.0V)	Figure 62
	BMOut	1 A (Battery Source)	6.1	0.15% (V_{BMOut}=4.0V)	Figure 59
	BMOut	1 A (Battery and USB source)	35.5	0.89% (V_{BMOut}=4.0V)	Figure 61

4.3.1 TLV62080 (3V3 Power Rail)

Perhaps the most important power rail to monitor the ripple and noise on is the TLV62080 3V3 as it will be powering the system load. In this TI Design, the TLV62080 exhibits very low amplitude ripple. At a 125-mA load test, shown in Figure 48, the 3V3 rail's ripple is equal or less than the noise floor of the oscilloscope used for testing. Figure 49 shows low jitter on the switch node when using only one source. When using two sources during high current loads as shown in Figure 51, the battery in addition to the PWRin source, the SW node will exhibit more jitter as the input voltage is constantly changing to balance battery and PWRin sources. Even while using dual sources and full load current the ripple of the 3V3 rail stays beneath 0.75%.
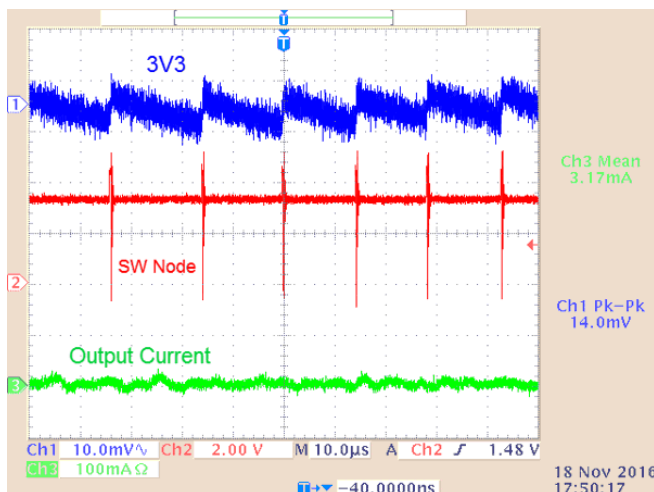
Figure 46. "3V3" Ripple (No Load; 24-V$_{AC}$ Source)
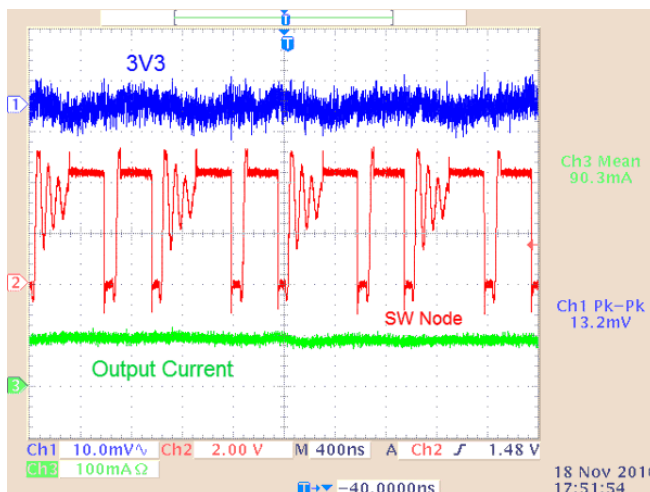
Figure 47. "3V3" Ripple (90-mA Load; 24-V$_{AC}$ Source)
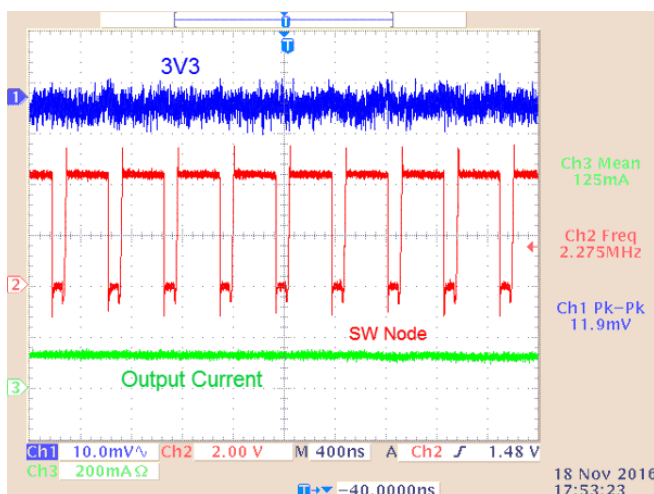
Figure 48. "3V3" Ripple (125-mA Load; 24-V$_{AC}$ Source)
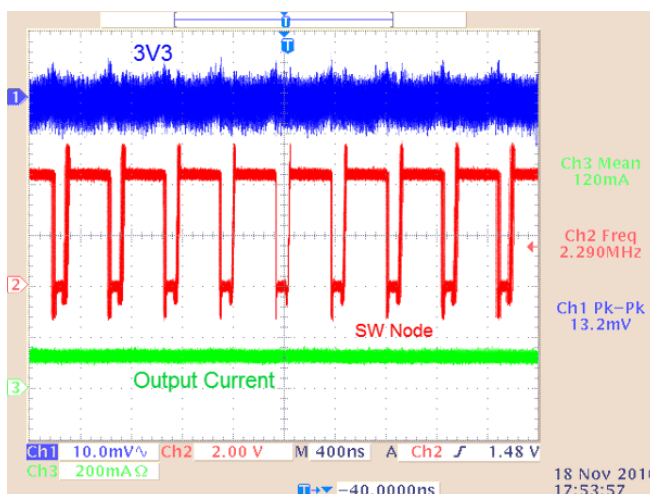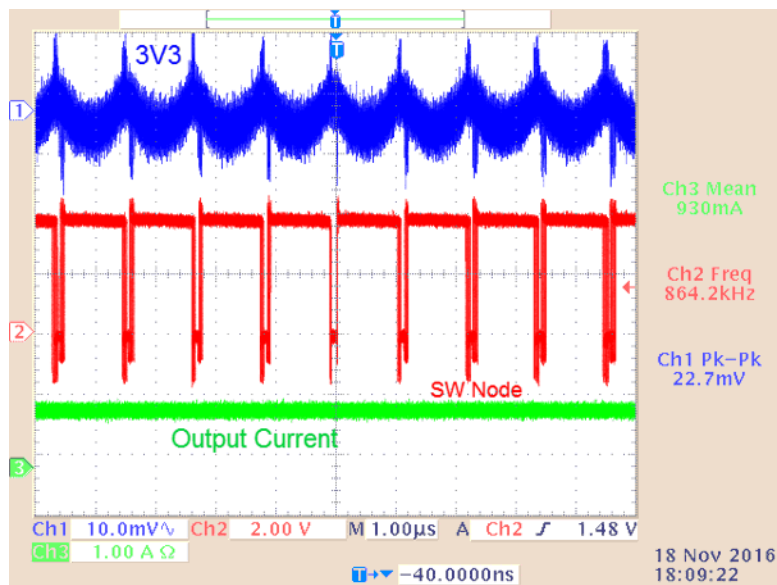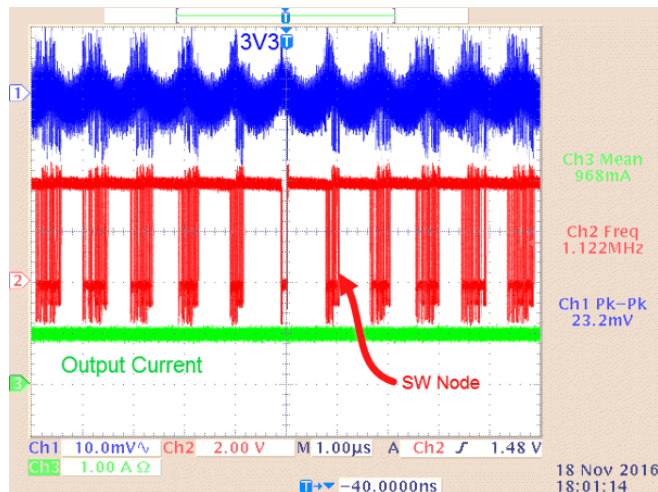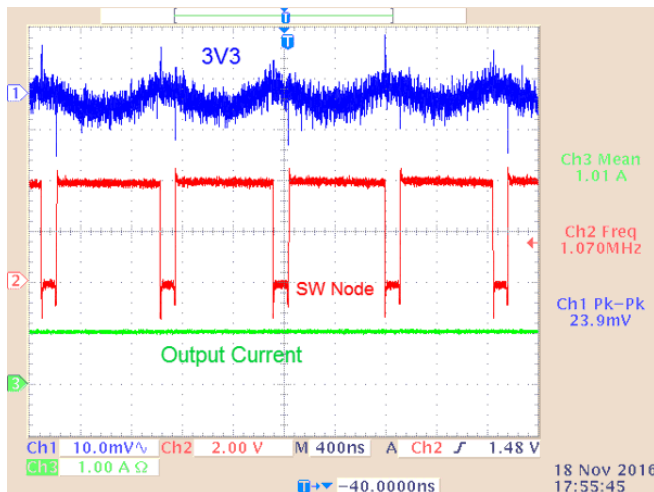
Figure 49. "3V3" Ripple Persist (120-mA Load; 24-V$_{AC}$ Source)

Figure 50. "3V3" Ripple (1-A Load; 24-V$_{AC}$ Source Plus Battery)

Figure 51. "3V3" Ripple Persist (1-A Load; 24-V$_{AC}$ Source Plus Battery)

Figure 52. "3V3" Ripple Persist (1-A Load; Battery Powered Only)

4.3.2   LM5166 (LMOut Power Rail)

The LM5166 produces a larger ripple when operating in DCM when compared to CCM. Regardless of the mode, the LM5166 produces an output ripple of less than 3% across the entire load range. Jitter on the switch node as shown in Figure 56 is expected as the rectified 24 V_{AC} exhibits significant ripple that the LM5166 is constantly adjusting for. The amount of ripple exhibited on the rectified 24 V_{AC} increases with higher load currents thereby increasing jitter on the LM5166 switch node.
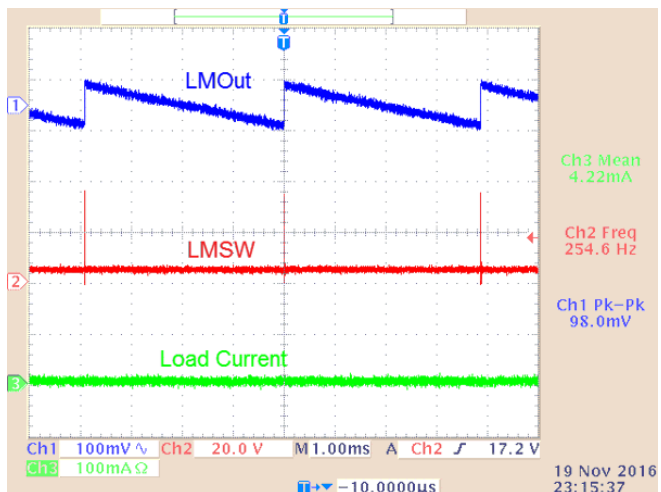
Figure 53. LMOut Ripple (No Load)
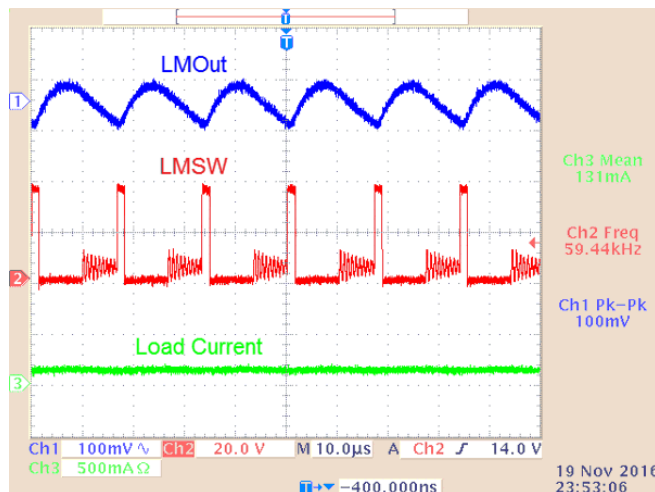
Figure 54. LMOut Ripple (130-mA Load)
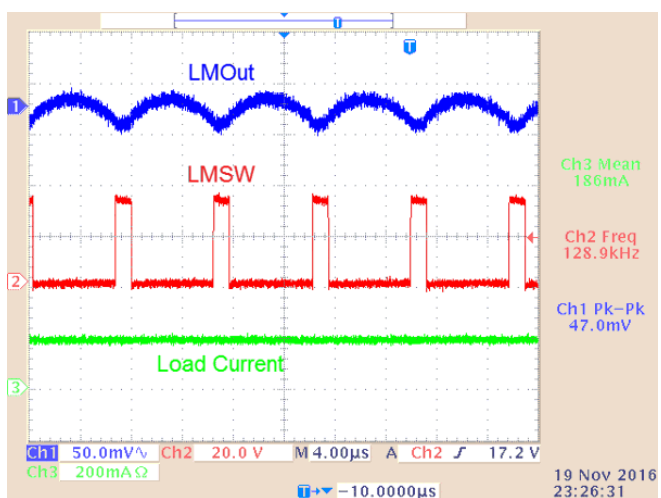
Figure 55. LMOut Ripple (180-mA Load)
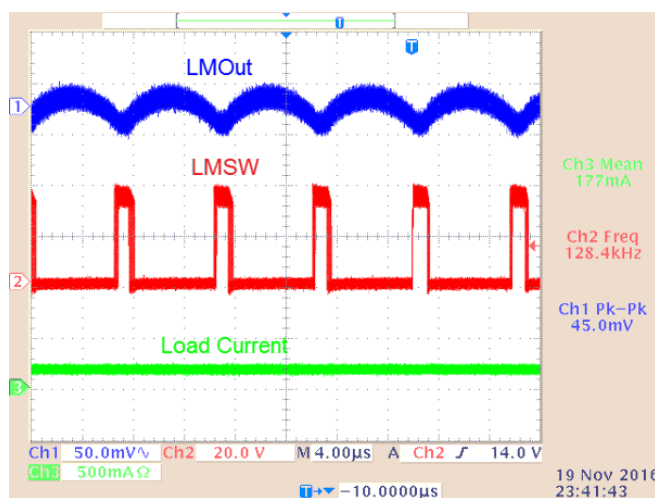
Figure 56. LMOut Ripple Persist (180-mA Load)
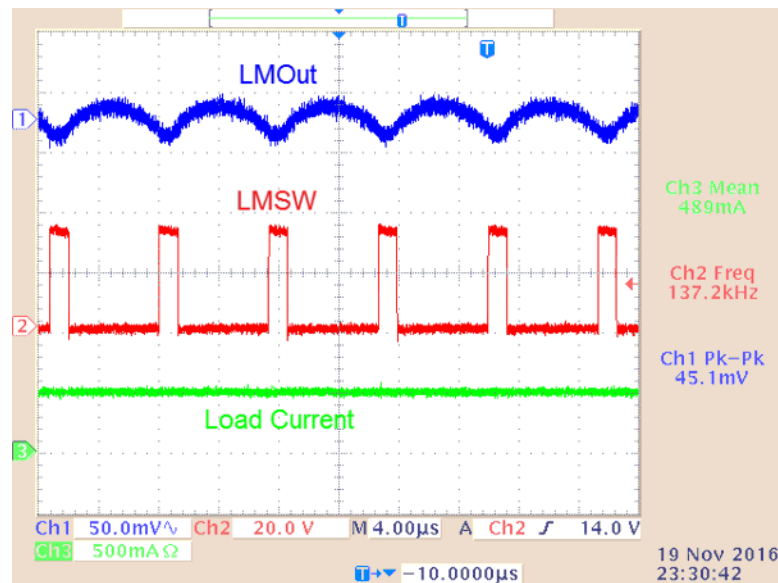
Figure 57. LMOut Ripple (490-mA Load)

4.3.3 BM24072 (BMOut Power Rail)

The ripple on the BMOut power rail varies significantly between battery usage only versus a PWRin source with battery power assist. When using only the battery, the BM24072 connects the battery to the output by closing an internal FET. As a result, the noise during purely battery operation is equal or less than the noise floor of the oscilloscope used for measurement. Figure 60, Figure 61, and Figure 62 show an increased ripple when using a source other than the battery.
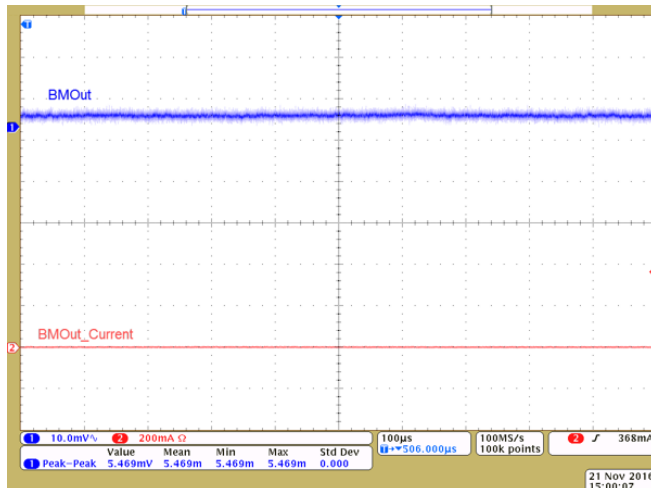
Figure 58. "BMOut" Ripple (0 A; Battery Source Only)
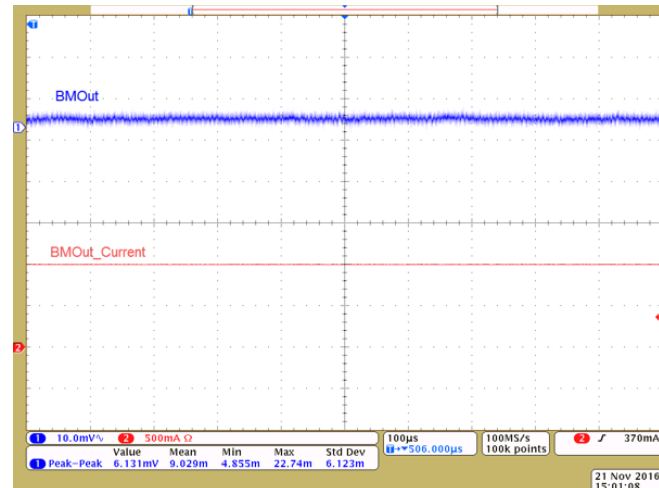
Figure 59. "BMOut" Ripple (1 A; Battery Source Only)
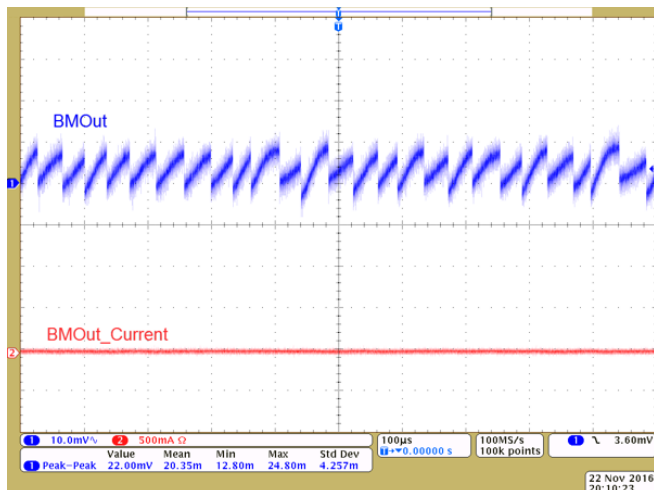
Figure 60. "BMOut" Ripple (1 mA; Battery and USB Sources)
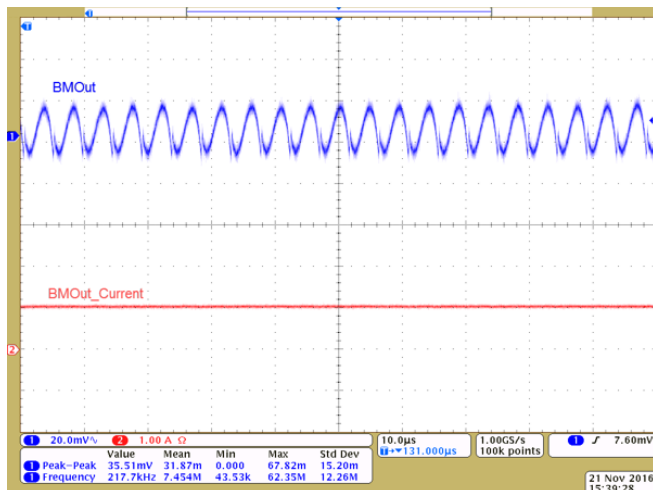
Figure 61. "BMOut" Ripple (1 A; Battery and USB Sources)
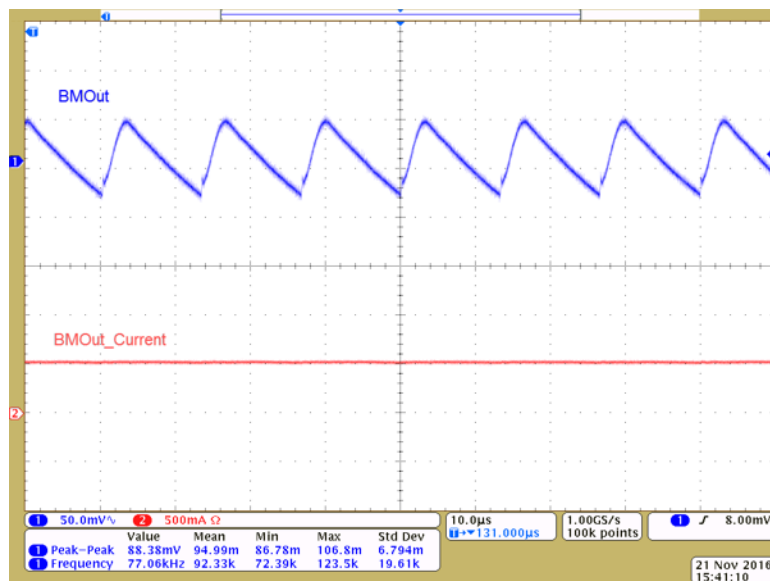
Figure 62. "BMOut" Ripple (500 mA; Battery and USB Sources)

24-V_{AC} Power Stage With Wide V_{IN} Converter and Battery Gauge Reference
Design for Smart Thermostats

4.4 Efficiency and Load Regulation

4.4.1 TLV62080

Efficiency on the BATT to 3V3 path is perhaps the most crucial as high efficiency on this path allows longer battery life and a smaller battery. The TLV62080 provides excellent efficiency, peaking at 96.6% efficiency at 165 mA at a nominal 3.7 battery voltage. The lower the battery voltage, the higher the efficiency of the BATT to 3V3 conversion. For this test, the input voltages were measured at C7 and the output voltages were measured at C10. The input current was fed at C7 and the output current to an electronic load was pulled from C10.
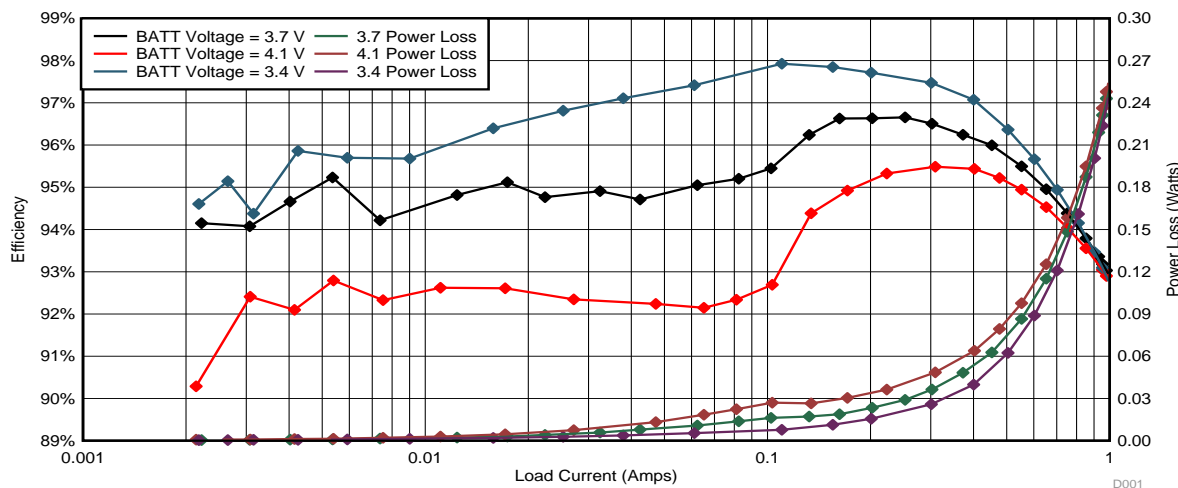
Figure 63. Battery to 3V3 Power Bus Efficiency and Power Loss
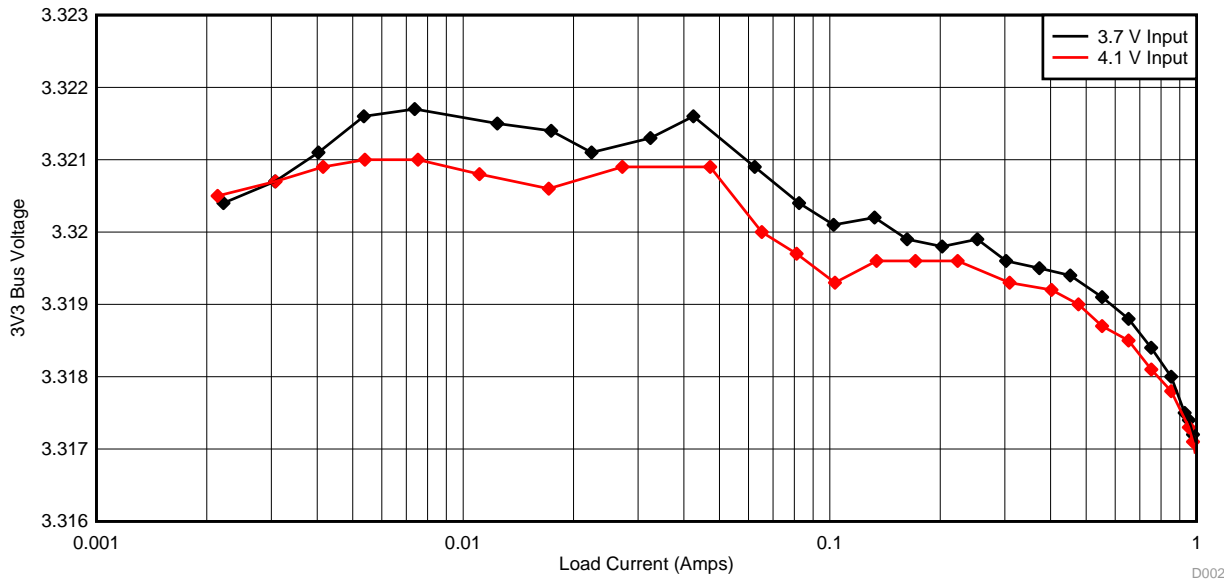
Figure 64. TLV62080 Load Regulation

4.4.2   LM5166

The LM5166 provides exceptional efficiency despite the large voltage difference between the input and output of the device. As with the BATT to 3V3 conversion, the efficiency of LM5166 increases as the input voltage decreases. The input voltage was measured at node RectOut side of R35 and the output voltage was measured at C23. The input current was fed through node RectOut and the output current was drawn from LMOut side of C23 and C24.
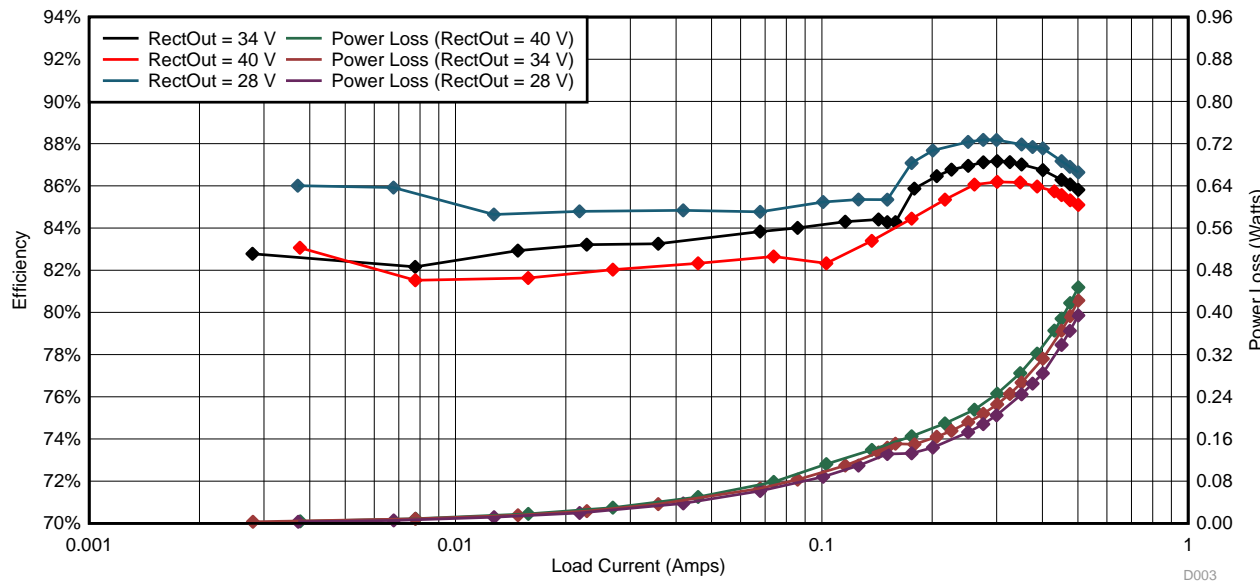
Figure 65. LM5166 Efficiency and Power Loss
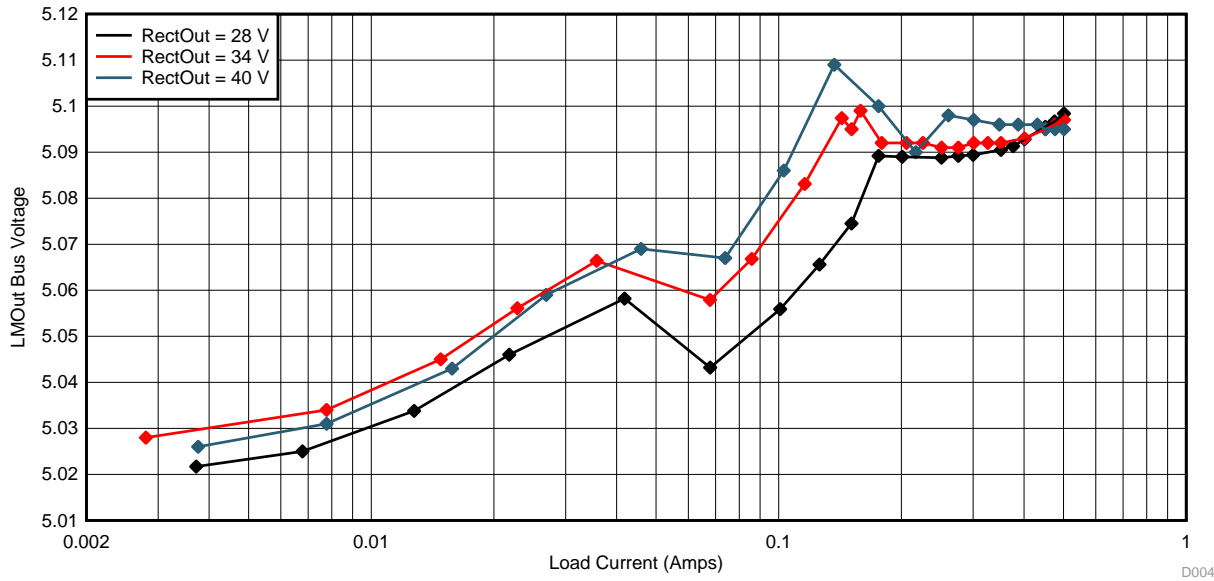
Figure 66. LM5166 Load Regulation

4.5   *Fuel Gauge Accuracy*

4.5.1   Linear Discharge From 100% to 0% SOC

This test case uses a linear discharge rate of 125 mA to bring the battery from a 100% SOC to 0%. Table 4 shows a worst case error of 1.077%, which is significantly less than pre-learning cycle max DOD error of 13.64% as shown in Section 3.2. This test shows that after a single learning cycle, as outline in Section 3.2, significantly improves the error and displays the easy-to-obtain accuracy of Texas Instruments Impedance Track without having to fully characterize a battery.

Figure 67 shows a comparison of the true relative state of charge (RSOC) and the RSOC as reported by the fuel gauge. The plot shows the gauge RSOC follows very closely along the true RSOC. The gauge RSOC is quantized to 1% increments. The true RSOC is calculated once the discharge has been completed and the true capacity based on integrating the passed charge throughout the discharge phase has been calculated. The true RSOC is then compared to the gauge RSOC to determine the gauge's reporting error. For step-by-step calculation procedures (including Excel-syntax equations) for calculating the error based on the test data, see the concise blog posts "How accurate is your battery fuel gauge? Part 1/2" and "How accurate is your battery fuel gauge? Part 2/2".

Figure 68 shows the remaining capacity of the battery and battery voltage versus time during the 125-mA linear discharge. The device was programed to display 0% SOC at a battery voltage of 3.35 V. This test verifies that battery capacity linearly decreases and hits 0% just as the battery voltage crosses 3.35 V. Figure 69 shows the battery voltage during just the discharge phase. Figure 70 displays a plot of the gauge's RSOC error through the discharge phase. The RSOC error zig-zags due to the 1% quantization.

Table 4. Fuel Gauge Test 1 Results Summary
(Linear Discharge)

PARAMETER	VALUE
Average error	0.095%
Worst error	1.077%
Error standard deviation	0.445%
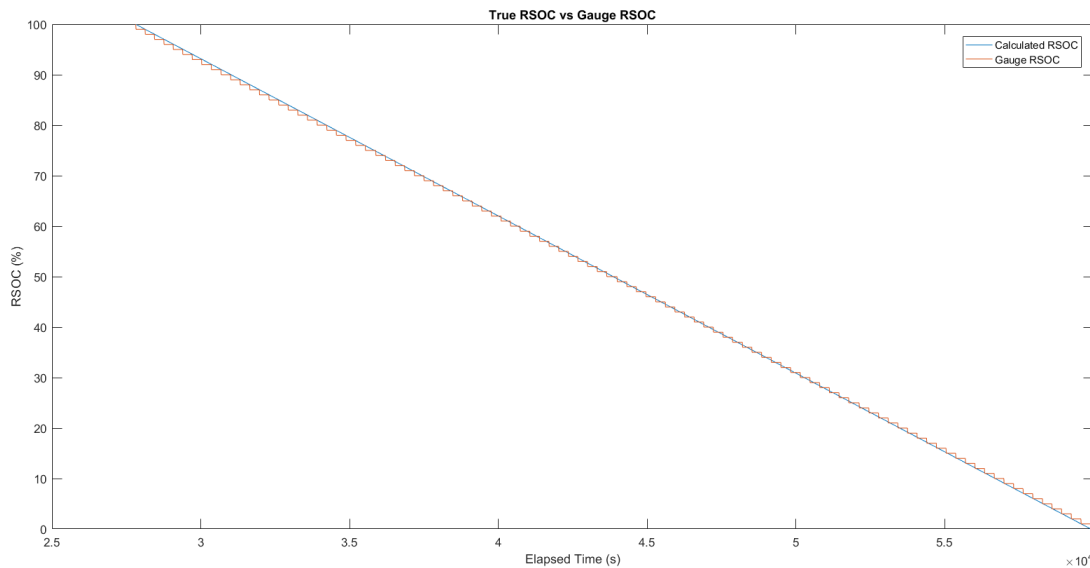
Figure 67. Relative SOC Comparison Plot (Linear Discharge)
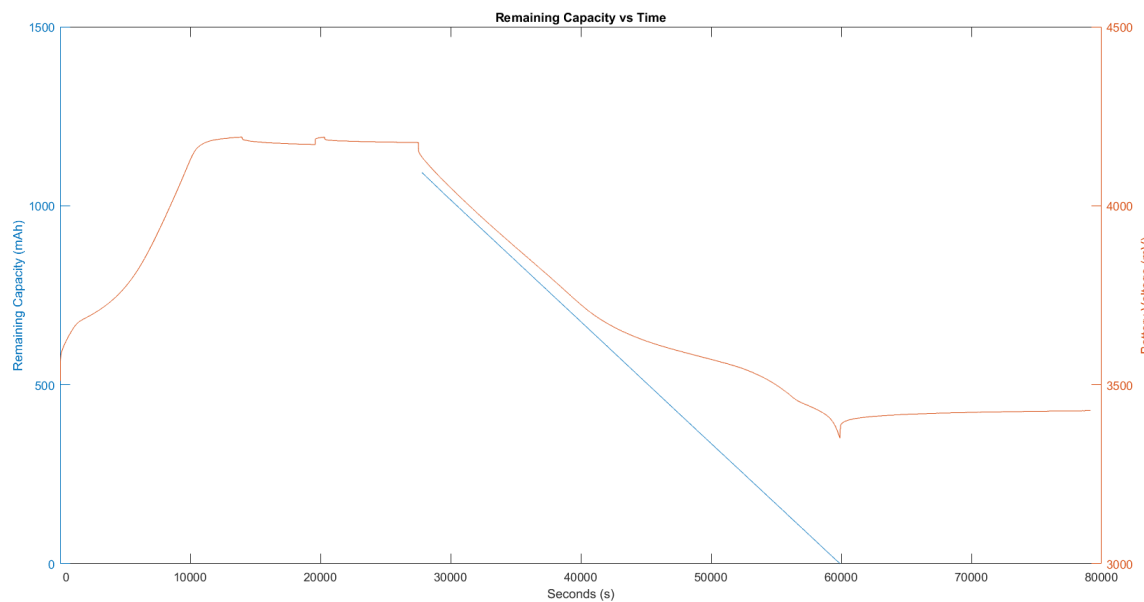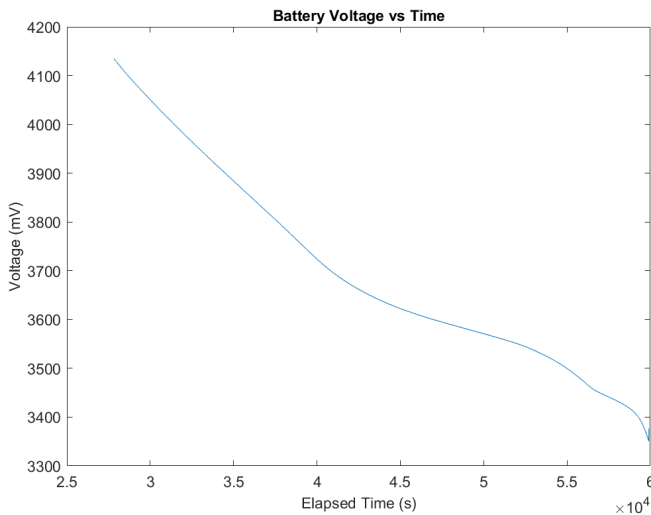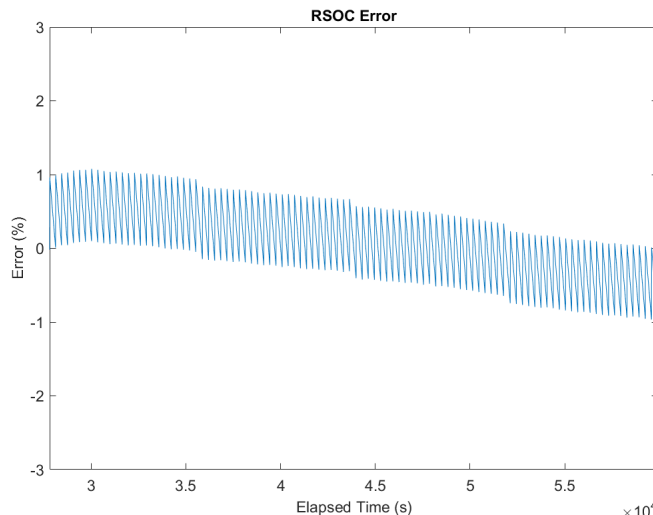
Figure 68. Remaining Capacity and Battery Voltage (Linear Discharge)

**Figure 69. Battery Voltage versus Time
(Linear Discharge)**

**Figure 70. Relative SOC Error versus Time
(Linear Discharge)**

4.5.2 Partial Charge-Discharge Cycles

The TIDA-01395 uses the battery for both backup and for power assistance. Even in the backup case, a brownout will not often last long enough for a battery to fully discharge. This test demonstrates the accuracy of the bq27426 fuel gauge when the battery undergoes partial charge-discharge cycles and when little to no rests between cycles are allowed. Typically, the accuracy of the fuel gauges will suffer under such circumstances. However, Table 5 shows the bq27426 fuel gauge still staying under 1% average error and under 2% maximum error.

Figure 71 shows the true SOC and the gauge reported SOC across three partial charge-discharge cycles. The reported SOC follows closely to the true SOC with the most error occurring when the battery is closest to the 100% SOC.

**Table 5. Fuel Gauge Test 2 Results Summary
(Charge-Discharge Cycles)**

PARAMETER	VALUE
Average Error	0.945%
Worst Error	1.954%
Error Standard Deviation	0.520%
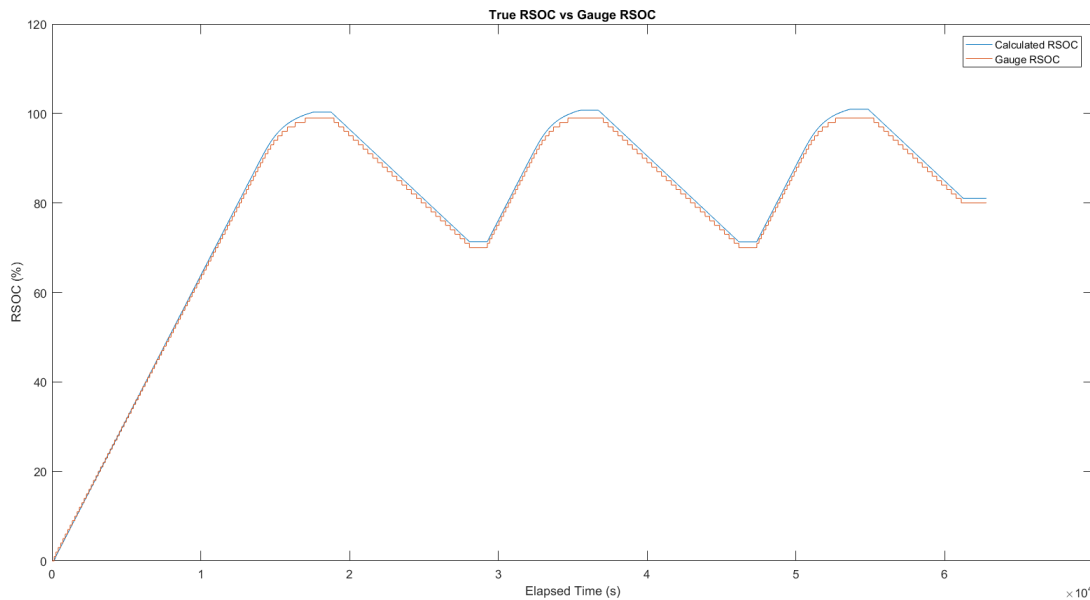
Figure 71. Relative SOC Comparison Plot (Charge-Discharge Cycles)
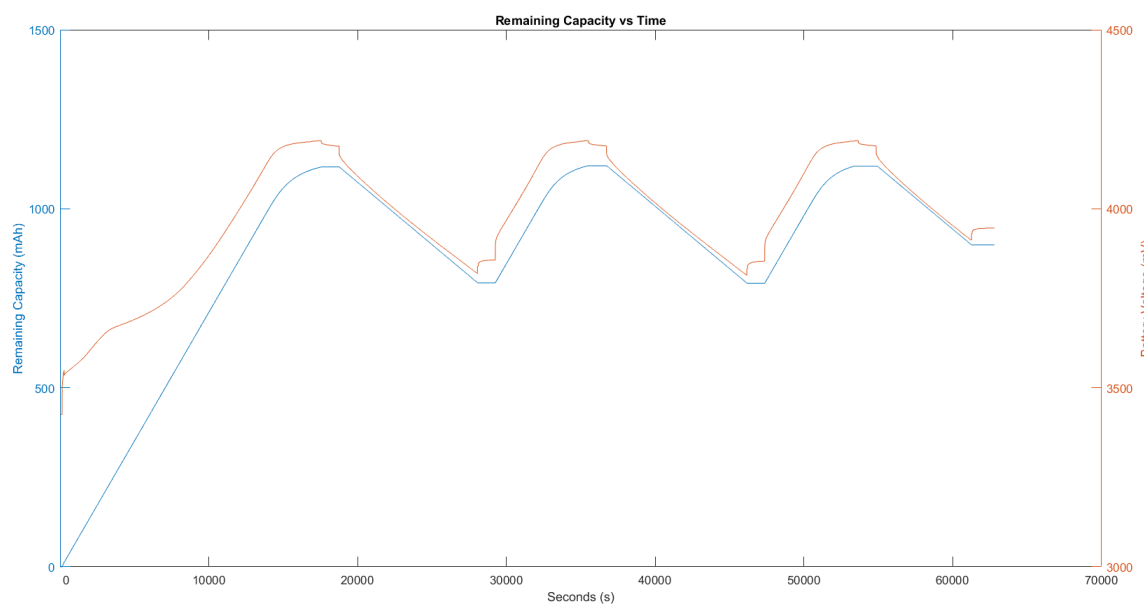
Figure 72. Remaining Capacity and Battery Voltage (Charge-Discharge Cycles)
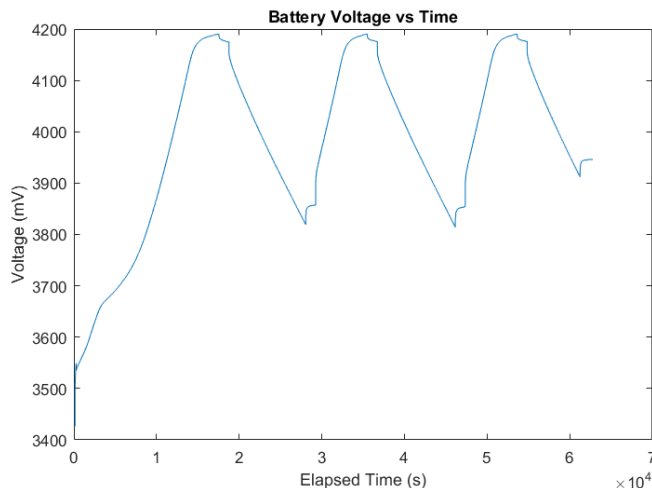
**Figure 73. Battery Voltage versus Time
(Charge-Discharge Cycle)**
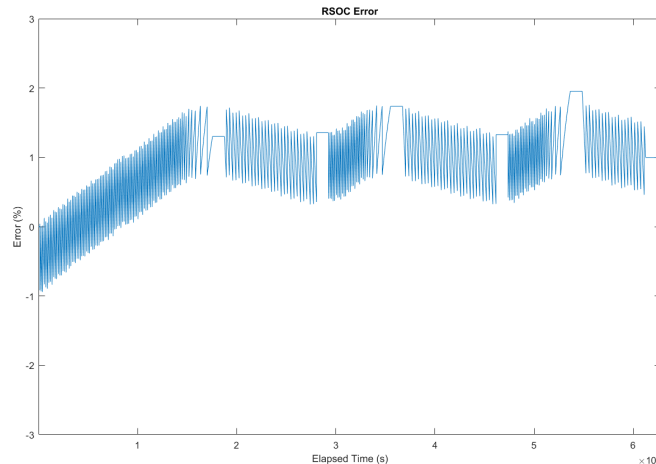
**Figure 74. Relative SOC Error versus Time
(Charge-Discharge Cycles)**

5 Design Files

5.1 *Schematics*

To download the schematics, see the design files at TIDA-01395.

5.2 *Bill of Materials*

To download the bill of materials (BOM), see the design files at TIDA-01395.

5.3 *PCB Layout Recommendations*

5.3.1 Layout Prints

To download the layer plots, see the design files at TIDA-01395.

5.4 *Altium Project*

To download the Altium project files, see the design files at TIDA-01395.

5.5 *Gerber Files*

To download the Gerber files, see the design files at TIDA-01395.

5.6 *Assembly Drawings*

To download the assembly drawings, see the design files at TIDA-01395.

6 Related Documentation

1. Texas Instruments, *Self-Powered AC Solid State Relay With MOSFETs Reference Design* , TIDA-00377 Design Guide (TIDUBR5)

2. Texas Instruments, *Low Cost AC Solid State Relay With MOSFETs Reference Design*, TIDA-01064 Design Guide (TIDUC87)

3. Texas Instruments, *Humidity and Temperature Sensor Node for Star Networks Enabling 10+ Year Coin Cell Battery Life*, TIDA-00374 Design Guide (TIDU797)

4. Texas Instruments, *Controlling Output Ripple and Achieving ESR Independence in Constant On-Time (COT) Regulator Designs*, Application Note (SNVA166)

5. Texas Instruments, *LM5166 3-V to 65-V Input, 500-mA Synchronous Buck Converter with Ultra-Low IQ*, LM5166 Datasheet (SNVSA67)

6. Texas Instruments, *bq2407x 1.5-A USB-Friendly Li-Ion Battery Charger and Power-Path Management IC*, bq24072 Datasheet (SLUS810)

7. Texas Instruments, *TLV6208x 1.2-A and 2-A High-Efficiency Step-Down Converter in 2-mm × 2-mm WSON Package*, TLV62080 Datasheet (SLVSAK9)

8. Texas Instruments, *TPS27081A 1.2-V to 8-V, 3-A PFET High-Side Load Switch With Level Shift and Adjustable Slew Rate Control*, TPS27081A Datasheet (SLVSBE9)

9. Texas Instruments, *LMx93, LM2903 Dual Differential Comparators*, LM2903 Datasheet (SLCS005)

10. Texas Instruments, *TPD2E2U06 Dual-Channel High-Speed ESD Protection Device*, TPD2E2U06 Datasheet (SLLSEG9)

11. Texas Instruments, *TPD1E10B06 Single-Channel ESD Protection Diode in 0402 Package*, TPD1E10B06 Datasheet (SLLSEB1)

12. Texas Instruments, *bq27426 System-Side Impedance Track™ Fuel Gauge*, bq27426 Datasheet (SLUSC91)

13. Texas Instruments, *Simple Guide to Chemical ID Selection Tool (GPC)*, Technical Reference (SLVA725)

14. Texas Instruments, *Achieving The Successful Learning Cycle*, Application Report (SLUA597)

15. Texas Instruments, *How accurate is your battery fuel gauge? Part 1/2*, TI E2E Community (http://e2e.ti.com/blogs_/b/fullycharged/archive/2016/09/26/how-accurate-is-your-gauge-part-1)

16. Texas Instruments, *How accurate is your battery fuel gauge? Part 2/2*, TI E2E Community (http://e2e.ti.com/blogs_/b/fullycharged/archive/2016/11/04/how-accurate-is-your-battery-fuel-gauge-part-2-2)

6.1 Trademarks

DCS-Control, Impedance Track, TINA-TI are trademarks of Texas Instruments.
Excel is a registered trademark of Microsoft.
All other trademarks are the property of their respective owners.

7 About the Author

CASSIDY AARSTAD is a systems designer at Texas Instruments, where he is responsible for developing reference design solutions for the industrial segment. Cassidy earned his master of science in electrical engineering (MSEE) from California Polytechnic State University in San Luis Obispo, California.